

Mineralogy and geochemistry of clay sediments in pans of the  
Northern Cape Province, South Africa.

by  
Tiani Roelofse

Submitted in fulfillment of the academic  
requirements for the degree of  
Master of Science in the  
School of Geological Sciences,  
University of KwaZulu Natal  
Durban

20 November 2010

As the candidate's supervisor I have approved this thesis for submission.

Signed: \_\_\_\_\_ Name: \_\_\_\_\_ Date: \_\_\_\_\_

## ABSTRACT

This thesis reports the results of a mineralogical and geochemical study of pans situated in the Northern Cape Province with special emphasis on the clay minerals. From east to west the depth and size of the pans increase and associated with this increased maturity the abundance of salt (halite and thenardite) and the quantity of green sediment are also enhanced. Chemically the sediments are dominated by  $\text{SiO}_2$  that also dilutes  $\text{Fe}_2\text{O}_3$ ,  $\text{K}_2\text{O}$ ,  $\text{Na}_2\text{O}$ ,  $\text{Al}_2\text{O}_3$  and  $\text{MgO}$  (when associated with dolomite) concentrations. Authigenic calcite, dolomite, analcime and loughlinite (Na-sepiolite) occur in some of the pans to the west and FTIR spectrometry indicates that all the pans host glauconite and/or celadonite. However, smectite, illite/smectite interstratification, kaolinite and/or chlorite and loughlinite only occur in some pans. The glauconite and/or celadonite does not occur as discrete mineral grains, but forms part of the fine-grained matrix common to all of the pans and no evidence of any precursor minerals were observed. The pan environment appears to present a closed, saline setting that is conducive for the direct precipitation of a mica with a chemical composition between that of glauconite and celadonite. The influence of the water-table on the formation of the glauconite and/or celadonite appears to be significant, as the highest abundance of salt is invariably associated with the position in the profile where the sediment appears to reach its most intense green colour. In the case of Koi Pan, the celadonite component of the solid solution seems to increase as the green colour intensifies. Loughlinite in Koi Pan and Brak Pan sediments also appear to be authigenic and it is suggested that it forms after precipitation of low Mg calcite that leads to Mg enrichment of the system and consequent sepiolite formation associated with minor dolomite. Thermoluminescence ages obtained from the Koi Pan sediment range between 37ka and 48ka before present at a depth of ~120cm below the surface, while for Brak Pan, at roughly the same depth, an age of between 110ka and older than 150ka before present was obtained. This may suggest different sedimentation rates in the pans or much younger ages and thus faster formation of glauconite and/or celadonite in Koi Pan since it is suggested that the mineral is authigenic.

## **Preface**

The experimental work described in this thesis was carried out at the Council for Geoscience, Pretoria (unless stated otherwise), from March 2004 to April 2009, under the supervision of Dr. M. Cloete (CGS) and Professor J.N Dunlevey (University of Kwazulu Natal).

These studies represent original work by the author and have not otherwise been submitted in any form for any degree or diploma to any tertiary institution. Where use has been made of the work of others it is duly acknowledged in the text.

### **Declaration – Plagiarism**

I, Tiani Roelofse, declare that

The research reported in this thesis, except where otherwise indicated, is my own original research.

The thesis has not been submitted for any degree or examination at any other university.

This thesis does not contain other persons' data, pictures, graphs or other information, unless specifically acknowledged as being sourced from other persons.

This thesis does not contain other persons' writing unless specifically acknowledged as being sourced from other researchers. Where other written sources have been quoted, then:

Their words have been re-written but the general information attributed to them has been referenced

Where their exact words have been used, then their writing has been placed in italics and inside quotation marks, and referenced

The thesis does not contain text, graphics or tables copied and pasted from the Internet, unless specifically acknowledged, and the source being detailed in the thesis and the References section.

Signed.....

## TABLE OF CONTENTS

<b>ABSTRACT</b> .....	<b>I</b>
<b>PREFACE</b> .....	<b>II</b>
<b>DECLARATION – PLAGIARISM</b> .....	<b>III</b>
<b>1 INTRODUCTION</b> .....	<b>4</b>
<b>2 FIELD WORK</b> .....	<b>5</b>
<b>3 LITERATURE STUDY</b> .....	<b>7</b>
3.1 GEOLOGICAL SETTING.....	7
3.2 GENERAL ASPECTS OF PANS .....	8
3.3 SOME ASPECTS OF KALAHARI PANS .....	9
3.4 MINERALOGY OF PANS IN THE VICINITY OF THE STUDY AREA .....	10
3.5 GLAUCONITE.....	10
3.6 GLAUCONITE <i>VERSUS</i> CELADONITE.....	12
3.7 GLAUCONITE <i>VERSUS</i> FERRIC ILLITE .....	14
3.8 GLAUCONITIZATION.....	14
3.9 WORLD WIDE OCCURRENCE OF GLAUCONITE.....	15
3.10 OCCURRENCE OF GLAUCONITE IN SOUTH AFRICA.....	16
3.11 TERRESTRIAL GLAUCONITE.....	16
<b>4 LABORATORY METHODS AND PROCEDURES</b> .....	<b>19</b>
4.1 X-RAY DIFFRACTION (XRD) .....	19
4.1.1 <i>Sample preparation</i> .....	19
4.1.2 <i>Instrumentation</i> .....	20
4.2 FOURIER TRANSFORM INFRARED (FTIR) .....	20
4.2.1 <i>Instrumentation</i> .....	20
4.3 PETROGRAPHY AND SCANNING ELECTRON MICROSCOPY (SEM) .....	20
4.3.1 <i>Sample preparation</i> .....	21
4.3.2 <i>Instrumentation</i> .....	21
4.4 X-RAY FLUORESCENCE (XRF) .....	21
4.4.1 <i>Sample preparation</i> .....	21
4.4.2 <i>Instrumentation</i> .....	21
4.5 INDUCTIVELY COUPLED PLASMA MASS SPECTROMETRY (ICP-MS) AND ION CHROMATOGRAPHY (IC).....	21
4.5.1 <i>Analytical procedure</i> .....	21
4.5.2 <i>Instrumentation</i> .....	22

4.8 THERMOLUMINESCENCE AGE MEASUREMENTS (TL).....	22
4.8.1 Analytical procedure .....	22
<b>5 RESULTS.....</b>	<b>24</b>
5.1 KOI PAN.....	24
5.1.1 XRD .....	26
5.1.2 FTIR.....	27
5.1.3 Petrography and SEM .....	29
5.1.4 XRF .....	38
5.1.5 TL age measurements .....	38
5.2 GAI GAI PAN.....	38
5.2.1 XRD .....	39
5.2.2 FTIR.....	40
5.2.3 Petrography and SEM .....	41
5.2.4 XRF .....	45
5.3 BRAK PAN.....	45
5.3.1 XRD .....	47
5.3.2 FTIR.....	47
5.3.3 Petrography and SEM .....	49
5.3.4 XRF .....	53
5.3.5 TL age measurements .....	53
5.4. OPSTAAN PAN.....	53
5.4.1 XRD .....	54
5.4.2 FTIR.....	55
5.4.3 Petrography and SEM .....	56
5.4.4 XRF .....	59
5.5 SOUT PAN .....	59
5.5.1 XRD .....	59
5.5.2 ICP-MS and IC .....	60
5.6 GAMMATEEP PAN .....	60
5.6.1 XRD .....	60
5.6.2 FTIR.....	60
5.6.3 Petrography and SEM .....	62
5.6.4 XRF .....	65
5.6.5 ICP-MS and IC .....	65
5.7 PALAEO MOLOPO RIVER BED.....	65
5.7.1 XRD .....	65
5.7.2 FTIR.....	65
5.8 ADDITIONAL DATA.....	66

<b>6 DISCUSSION .....</b>	<b>70</b>
6.1 KOI PAN.....	70
6.2 GAI GAI PAN .....	72
6.3 BRAK PAN.....	72
6.4 OPSTAAN PAN.....	73
6.5 SOUT PAN .....	74
6.6 GAMMATEEP PAN .....	74
<b>7 CONCLUSIONS.....</b>	<b>75</b>
<b>8 ACKNOWLEDGEMENTS .....</b>	<b>79</b>
<b>9 REFERENCES .....</b>	<b>80</b>

### **Appendices**

Appendix A. Location and description of samples

Appendix B. X-Ray Diffraction data

Appendix C. Scanning Electron Microscope data

Appendix D. X-Ray Fluorescence data

Appendix E. Inductively Coupled Plasma Mass Spectrometry and Ion Chromatography data.

## 1 Introduction

In geomorphology the term 'pan' is used to describe a shallow body, normally rounded or ellipsoid, of often saline water found in arid regions that during the dry season dries out completely or has a greatly reduced water content. These features are called playas, or playa lakes, in the south western USA and salinas in Spanish speaking countries (Bates and Jackson 1983). In South Africa the highest concentration of pans occurs in the arid interior of the Cape Province in areas composed of unconsolidated Kalahari sands or Ecca and Dwyka Group sediments of the Karoo Supergroup (Goudie and Thomas 1985). The pans investigated in this study are all situated in these lithologies in the most north-western part of the Cape Province between 27° 30' and 28° 00' South and 20° 00' and 22° 30' East (Fig. 1); an area which is generally referred to as the southern Kalahari (Thomas and Shaw 1991) which receives less than 200mm annual rainfall and has a mean maximum summer temperature of 35°C. Reports of a green colour associated with the sediments in some Kalahari pans and the tentative identification of glauconite as the mineral responsible for this colouration initiated a detailed investigation, as the IMA classification of the Mica Group (Rieder *et al.* 1998) has placed a rigid definition on the mineral glauconite. Furthermore, in parallel with this more detailed understanding of the structure and chemistry of the Mica Group the concept has developed that the genesis of glauconite is restricted to shallow marine environments (McRae 1972; Velde 1992). Rogers (1937) reported a fine-grained green material in several Kalahari pans, and although not identifying the mineral species, recorded that it was also present in sediments of the Kalahari System as well as clasts of the older granite, schist and quartzite in the pans' sediments. Du Toit (1954) also mentioned that the floors of pans in the Kalahari Region were composed of greenish coloured sandstone. The first detailed work on the pans' sediments was that of Boocock and van Straten (1962) who identified the greenish clay mineral present in some of the saline pans as glauconite. Netterberg (1969) also reported the presence of glauconite in various dolocretes, calcretes, silcretes and argillaceous sediments from pans in the Kalahari, and Buhmann *et al.* (1999) noted large quantities of glauconite in Heunningsvlei Pan, although this site is to the east of the study area some 175 km north of Vryburg (Fig. 1) in the North West Province. Unfortunately, details of the parameters used to classify the green materials as glauconite are not given in the pre 1980 publications, and in view of the recently developed more rigid classification of the Mica Group (Rieder *et al.* 1998) these identifications should be regarded as tentative.

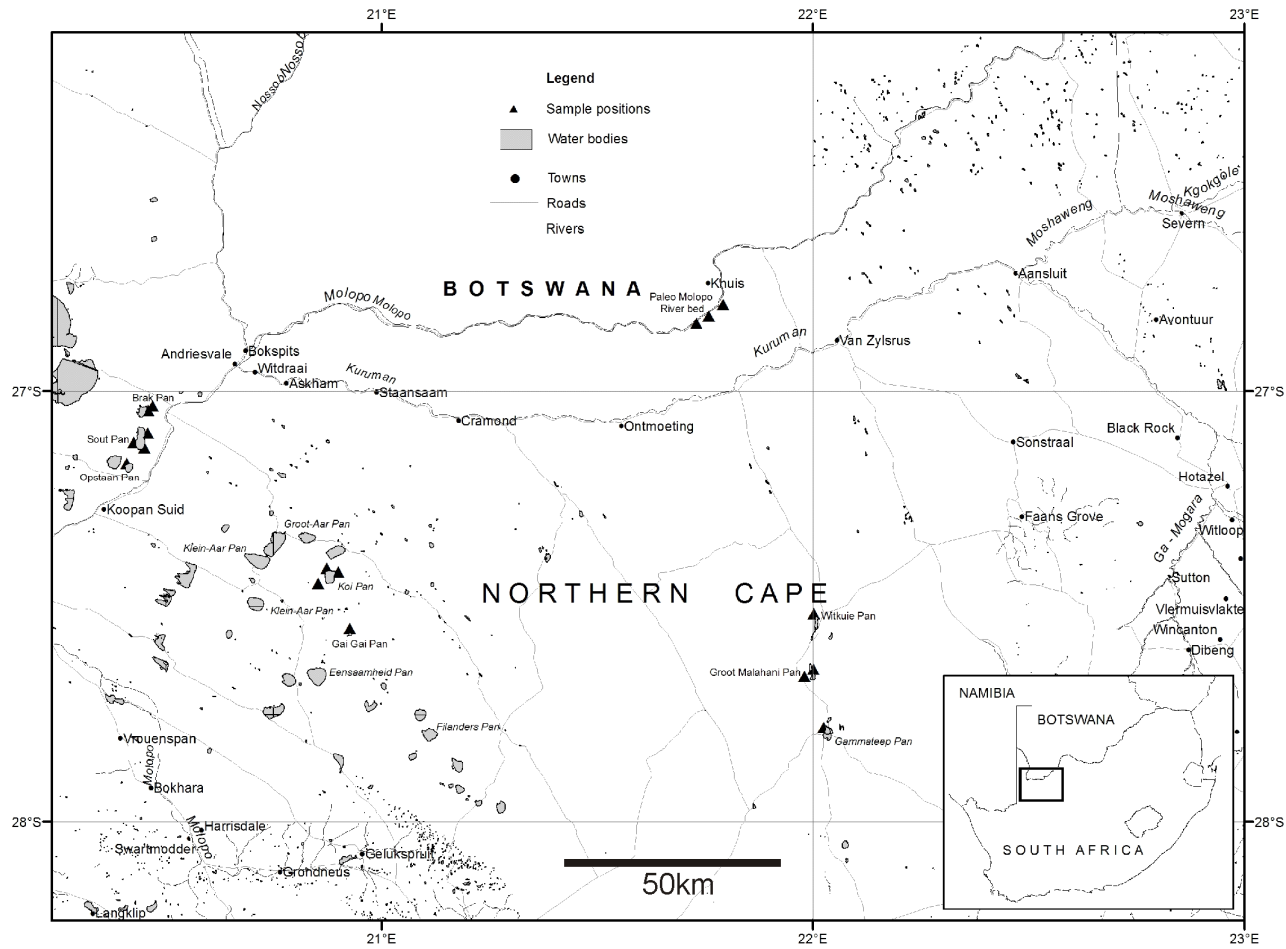


Figure 1. Map of the study area and localities of pans under investigation.

The primary objective of the study was to establish the chemical and mineralogical composition of the green coloured sediments associated with the large swarm of pans north west of Upington in order to unequivocally establish the identity of the green mineral and develop a geochemical model for the authigenic formation from the detrital material. The pans selected for detailed study are shown in Fig. 1 and details given in Table A1 of Appendix A. Although there is a very high concentration of pans, over 90% of the study area is covered by the red aeolian sands of the Gordonia Formation (Kalahari Group) which has a maximum thickness of some 110m where troughs in the pre-Kalahari land surface have been filled. The red sands of the Gordonia Formation form longitudinal dunes, with pans developed in the depressions between the dunes. Most pans are small and shallow, but some are up to 20km in diameter with floors 30m below the maximum fill surface. Brak Pan is typical of the larger pans and the photograph (Fig. 2) shows the generally arid nature of the environment with the pan in the hollow between two vegetated longitudinal dunes. Several of the pans in the Kalahari produce salt deposits during the dry season (Oosterhuis 1998) that are exploited as a source of halite by companies such as Saltcor Pty. The pans Opstaan Pan and Sout Pan (Figs. 3 and 4) on the farm Zout Pan 222 in the study area are presently (2008) actively being exploited.



*Figure 2. Brak Pan on the farm Zout Pan 222. Photograph taken from the top of a dune on the eastern side of the pan with the vegetated dune on the western side of the pan visible in the background.*



*Figure 3. Opstaan Pan on the farm Zout Pan 222. The piles of halite produced by crystallization of brine concentrated by solar evaporation are clearly visible.*



*Figure 4. Sout Pan on the farm Zout Pan 222. The thick crust of salt is visible in the foreground and the bakkie (center frame close to the 'shoreline') illustrates the height of the dunes that surround the pan.*

## 2 Field work

Pan sediments were collected using a hand-held stainless steel bucket auger at approximately 20cm intervals down to 1m below the surface (Fig. 5). Dark green material was common below the light brown surfaces. pH measurements were determined in the field and afterwards in the laboratory using the soil paste method. Phenolphthalein was also used in the field to estimate the pH values of pan sediments. Other green material in the vicinity of the pans were also sampled and these included conglomerate (grit), in the vicinity of Gai Gai Pan, that displayed a green alteration zone on the outer margin of the sample (Fig. 6). Samples of green sandstone and shale displaying mud cracks were collected in the palaeo Molopo River bed (Fig. 7).



*Figure 5. Green pan sediment taken at a depth of ~20cm below the surface of Koi Pan (situated on the farm Zout Pan, 222, Kalahari)*



*Figure 6. Conglomerate (grit) found in Gai Gai Pan showing a green alteration zone on the outer margin of the rock.*



*Figure 7a. A cliff that forms part of the palaeo Molopo River bed (see Figure 1) where green rocks are tumbling down the slope of the hill. 7b. Closer inspection of the exposed rocks revealed mud cracks preserved in olive green sandstone.*

Three samples from Koi Pan and Brak Pan were collected for thermoluminescence age measurements by forcing a metal tube attached to a hand-held auger vertically into pan sediments at different depths. The samples were shielded from sunlight by using black bags, firstly to cover the auger holes during sampling and secondly to wrap the samples in afterwards. The samples were kept undisturbed in the metal tubes until the tests were performed.

### 3 Literature study

#### 3.1 Geological setting

The study area is part of the peneplain drained by the Molopo and Kuruman Rivers. Although some 90 per cent of the area is composed of aeolian sands of the Gordonia Formation (Kalahari Group), inliers of Karoo dolerite and kimberlite related to the ancient topography are present. Information from boreholes indicates that the units beneath the Gordonia Formation range from Tertiary to Mokolian in age with the Precambrian units having undergone extensive folding and deformation. In the overall stratigraphy the Kalahari Group sediments rest unconformably on the Karoo Supergroup which is separated from the younger units by an angular unconformity. The Neoproterozoic Nama Group as well as the the Koras, Wilgenhoutsdrif and Brulpan Groups (part of the Namaqua-Natal Province) are all extensively deformed. The Grobelershoop Formation (Brulpan Group) is considered to be the oldest unit in the area (~1 780ma) (Cornell *et al.* 2006). Although the geology of the study area is described in the 1:250 000 Noenieput (mapped by Thomas and Thomas 1989) and 1:250 000 Nossob and Twee Rivieren (mapped by Thomas *et al.* 1988) geologic maps, subsequent revision and reclassification has changed the status of certain stratigraphic units and thus the column presented in Fig. 8 represents a modification of previously published data (SACS 1980; Thomas *et al.* 1988; Thomas and Thomas 1989). The occurrence of pans in this area is mostly associated with palaeo drainage lines (Malherbe *et al.* 1986) and their sizes range from small depressions to those with diameters that measure in kilometers.

Quaternary		Kalahari Group	Pan Sediments		
			Gordonia Formation	Red and flesh coloured windblown sand	
Mokalanen Formation	Calcrete that is diatomaceous in places				
Tertiary	Eden Formation		Red, brown and green sandstone with sand-filled biotubes in places; calcareous grit; conglomerate		
	Budin Formation		Red to brown calcareous clay		
	Wessels Formation	Clayey gravel			
Jurassic		Intrusive rock	Dolerite		
Permian		Karoo Sequence	Ecca Group	Prince Albert Formation	Grey, green and brown shale (varved in places); sandstone, arkose, grit; lenses of impure limestone
Carboniferous			Dwyka Formation	Tillite; shale, brown grit and conglomerate; impure brown limestone and calcarenite	
Namibian		Nama Group	Nababis Formation	Red, brown, black and green cross-bedded sandstone, flagstone, shale	
			Breckhorn Formation	Purple, red and brown cross-bedded sandstone and flagstone; clay pellet conglomerate	
Mokolian		Koras Group	Steenkamspuits Formation	Red quartz-feldspar porphyry	
			Wilgenhouts drif Group	Zonderhuis Formation	Massive purple quartzite
		Olifantshoek Sequence	Groblershoop Formation	White quartzite, quartz-muscovite schist	

Figure 8. Stratigraphic column of rocks and sediment in the study area.

### 3.2 General aspects of pans

The origins of pans are widely debated and views range between the importance of influences from animal erosion, termites, aeolian deflation, salt weathering, topography and bedrock. Thomas and Shaw (1989) have listed the following general characteristics of a pan or playa: They occupy regional or local topographic lows; they lack surface inflows; they are occupied by ephemeral water bodies; they usually have flat surfaces; they have a hydrological budget in which evaporation greatly exceeds inputs; they have vegetation-free surfaces or, where vegetation occurs, distinct vegetation associations. After taking the various views into account Goudie and Thomas (1985), proposed the model of pan formation illustrated in Fig. 9.

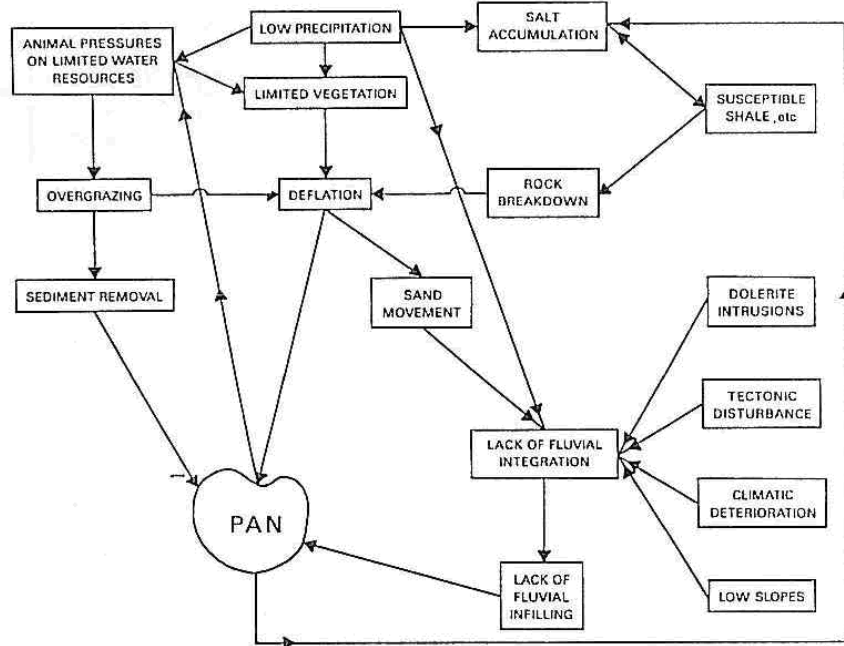


Figure 9. A flow diagram showing possible pathways of pan formation (After Goudie and Thomas 1985).

Goudie and Thomas (1985) stated that miscellaneous factors could be important for the formation of pans, and proposed that in areas with a dry climate, and thus low vegetation, the movement and growth of dunes could lead to the blocking of drainage and localised accumulation of water. This localised water and salt development would in turn lead to localised animal activity etc. Pans are commonly associated with features such as palaeo-drainage lines, dolerite dykes or tectonic deformation that lead to the disruption of drainage, but they can also form in areas with little fluvial integration, where deflation and animals do not play a role. Solution of dolomitic rocks or meteorite impacts may also lead to the formation of pans (Goudie and Thomas 1985). The sediments in pans are dominantly fine-grained and mainly brought in by surface flow, while other constituents include solutes and organic materials. In addition to silica, the main ions found in pan environments are  $\text{Ca}^{2+}$ ,  $\text{Mg}^{2+}$ ,  $\text{K}^+$ ,  $\text{Na}^+$ ,  $\text{Cl}^-$ ,  $\text{HCO}_3^-$ ,  $\text{CO}_3^-$  and  $\text{SO}_4^{2-}$  which are derived from the surface and groundwater catchments (Thomas and Shaw 1989). Saline minerals are formed from the evaporation of surface brines and subsequently, after the water-table has dropped below the surface, from interstitial capillary evaporation (Eugster and Kelts 1983).

### 3.3 Some aspects of Kalahari pans

According to Goudie and Thomas (1985), most of the southern Kalahari pans occur on the

arid side of the 500mm isohyet and 1 000mm free evaporation isoline. Wind erosion plays an important role in the development of the pans as sand is transported from and over the pan floor by the prevailing winds that deposit it on the lee side building a sand ridge. After cycles of deposition of sediment from the surrounding area and aeolian activity, fine-grained sediment accumulates and forms impermeable layers which are conducive for the formation of pans. Boocock and van Straten (1962) stated that the saline pans in the Kalahari are progressively being extended at the present time, and that the clay minerals present on the pan floors are saturated with respect to sodium and therefore when dry, possess a flocculated structure that inhibits their removal by wind activity. Some of the larger pans in the Kalahari have a tectonic origin and were enhanced by deep weathering processes and ground water activity (Thomas and Shaw 1991); however, the pans under investigation all show a relationship to the old river drainages as observed by Malherbe *et al.* (1986).

#### 3.4 Mineralogy of pans in the vicinity of the study area

Previous work on pans from the same general area includes that by Mees (2001) who studied Otjomongwa Pan situated in the south-western Kalahari, Namibia. Mees (2001) reported mineral assemblages that include quartz, calcite, and dolomite with large quantities of Mg-smectite with some mica and sepiolite in the clay fraction. Mees (2003) also reported the salts thenardite, halite and minor amounts of gypsum, eugsterite and glauberite in this pan. For the specific pans investigated in this study no reports of previous mineralogical or geochemical work could be found in the literature.

#### 3.5 Glauconite

Because one of the main foci of the study was to verify the presence of glauconite in the pans, the mineralogy and chemistry of glauconite will be discussed in detail together with related minerals such as celadonite and ferric illite that are very similar to glauconite in terms of their chemistry and crystallographic structure.

The 1978 AIPEA Nomenclature Committee defined glauconite as a Fe-rich dioctahedral mica with tetrahedral Al (or Fe<sup>3+</sup>) usually greater than 0.2 atoms per formula unit and octahedral R<sup>3+</sup> correspondingly greater than 1.2 atoms. Opinions on the crystal structure and the octahedral occupancy vary in the literature, and the main similarities and discrepancies are briefly discussed below. Odom (1984) classified glauconite as a dioctahedral, hydrous iron and magnesium aluminosilicate mica with the basic unit structure consisting of a 2:1 layer sequence bonded together by interlayer K cations. Most authors (e.g. Gruner 1935; Kossovskaya and Drits 1970; Millot 1970) support a dioctahedral unit structure, but some

authors, such as Jarrar *et al.* (2000) support a trioctahedral unit structure. There is, however, chemical (Odom 1984) and crystallographic (Weaver and Pollard 1973) evidence that indicates that the structure of glauconite lies between that of a dioctahedral and a trioctahedral mica. Possible reasons for the expanding of the unit cell from dioctahedral to an intermediate value, between di- and trioctahedral are -

- 1 substitution of the Al ion for the much larger Fe ion, which stretches the unit cell in the b direction (Weaver and Pollard 1973).
- 2 the occurrence of trioctahedral sheets amongst dioctahedral sheets (Bentor and Kastner 1965).

The crystal structure of glauconite can be considered similar to that of biotite (Deer *et al.* 1996; Jarrar *et al.* 2000) or illite (Odom 1984; Manghani and Hower 1964; Millot, 1970), and interstratified illite/smectite layers within the structure are confirmed by various authors (Manghani and Hower 1964; Weaver and Pollard 1973; Bailey 1980; Odom 1984).

The colour of glauconite can range between colourless, yellowish green, green and blue-green, and as the glauconitization process progresses the green colour intensifies (Ehlmann *et al.* 1963; McRae 1972; Odom 1984). Glauconite usually appears green in thin section (Deer *et al.* 1996).

According to Odin and Matter (1981) the basal reflection of glauconite, when analysed by means of XRD, can be anywhere between 14 and 10Å depending on the maturity of the mineral, but for most glauconite samples the 10Å, mica, layers dominate and the amount of expandable layers ranges from <5 to approximately 55% (Manghani and Hower 1964). The glauconite peak is usually asymmetrical with a broad base except when situated at 10Å when the peak is sharp (Odin and Matter 1981). A decrease in sharpness (width at ½ height) and a shift of the basal reflection to higher d-values are directly related to the decrease of the potassium content, and an increase in the amount of expandable layers. This process is accompanied by a colour change in the mineral from dark to pale green (Ehlmann *et al.* 1963; Odom 1984). The basal reflection hardly changes position after glycol solvation, except when cation exchange of potassium is performed (Odin and Matter 1981) and a peak shift from 14Å to 17Å, after treatment with ethylene glycol, proves the presence of swelling layers (Odin and Matter 1981).

Burst (1958), Hower (1961) and Bentor and Kastner (1965) classed glauconite pellets as: ordered, disordered, interstratified glauconite-smectite. Burst (1958) and Bentor and Kastner

(1965) further recognise in their classification that pellets may contain glauconite in one of the mineralogical forms mixed with clay or none-clay minerals and green pellets containing none of the mineralogical forms of glauconite. Also more than one mineralogical form of glauconite may be present in a single bulk sample (Odom 1984).

### 3.6 Glauconite *versus* celadonite

Glauconite and celadonite form separate mineral species, but considerable overlap in their chemistry can occur (Buckley *et al.* 1978) and a continuous series probably exists between these minerals (Slonimskaya 1986) making differentiation difficult. The main chemical differences include the lower aluminum tetrahedral content (Buckley *et al.* 1978) and the lower Fe/Mg ratio in celadonite (Millot, 1970; Buckley *et al.* 1978). The magnesium content of celadonite usually ranges between 5-9% compared to the 2-3% of glauconite (Hendricks and Ross 1941). Related to the aluminum content is the slightly higher silica content of celadonite that ranges between 52-56% (Odin and Matter 1981). Other differences include celadonite usually having a higher potassium content (Buckley *et al.* 1978).

While celadonite is associated with igneous rocks where it commonly occurs as vesicular cavity fillings of basalts, or to a lesser extent as the replacement product of olivine and hypersthene (Odin *et al.* 1988), glauconite is strongly associated with a marine environment with a slow sedimentation rate. Table 1 highlights the main differences and similarities between the environments and conditions that may lead to the formation of glauconite and celadonite as discussed by Odin (1988). The physical environment that favours the formation of glauconite is colder, and probably has a lower pressure than that required for celadonite formation, but besides these factors both minerals require a quiet, saline environment. Chemically both glauconite and celadonite require ion rich fluids to form, but while glauconite usually develops from a pre-existing substrate by successive reactions, celadonite precipitates from fluids in a single reaction leaving much finer grains than in the case of glauconite. A strong association between celadonite and zeolites is noted, while, in contrast to this, glauconite shows no association with zeolite minerals.

Table 1. A comparison between the environments that favour the formation of glauconite and celadonite, respectively.

<b>Glauconite</b>	<b>Celadonite</b>
<i>Physical environment</i>	
saline	saline
slow sedimentation rates	deep sea
below 15°C or even 10°C	20°C (50-90°C)
pH 7-8	
oxidising and reducing conditions in presence of organic material	oxidising and reducing conditions
shells provide closed environment with local reducing conditions	needs confined spaces to minimise dilution of fluids
concentrated on continental shelf areas, fairly shallow waters, from variety of starting material by marine diagenesis.	From volcanic rock at sea bottom
<i>Chemical environment</i>	
availability of K and Fe in pore fluids, sea water travels short distance ~ sea water composition not changed much	grow from very ion rich fluids- sea water travels deep through fractures and are modified by rock before reaching the void where mineral precipitates
forms from successive reactions: Fe-rich smectite-recrystallization processes which trap more and more K	forms in equilibrium with circulating fluid in a single reaction
develops in micropores from substrate	develops in voids
microcrystals larger; occurs as grains	microcrystals smaller; never occurs as grains
<i>Associated minerals</i>	
no association with zeolites; associated with pyrite	associated with smectite and zeolites

### 3.7 Glauconite versus ferric illite

Mineralogically and chemically, ferric illite is very similar to glauconite and the only difference, according to Odin and Matter (1981), is the higher content of iron in glauconite: on average 5% Fe<sub>2</sub>O<sub>3</sub> for illite versus 23% Fe<sub>2</sub>O<sub>3</sub> for glauconite (Srodon and Eberl 1984). Hillier (1995) concluded that the ferric iron content of non-marine glauconite is intermediate between glauconite and illite i.e. around 10% Fe<sub>2</sub>O<sub>3</sub>. Crystallographically glauconite and illite are identical (Odin and Matter 1981), but the size of the (002) reflection can be used to distinguish between illite and glauconite: as glauconite has a very low intensity ratio (002) reflection, due to the high amount of iron in the octahedral position, compared to illite (Moore and Reynolds 1997). In contrast to the marine origin of glauconite, ferric illite is believed to be indicative of a restricted hyper-saline environment (Kossovskaya and Drits 1970).

### 3.8 Glauconitization

Glauconite is formed from a variety of starting materials by marine diagenesis, usually in fairly shallow waters with reducing conditions in the presence of organic material (Deer *et al.* 1996). According to Velde (1992) the genesis of glauconite is confined to the sediment-seawater interface with a low sedimentation rate. Weaver and Pollard (1973) believed that a saline, oxidising environment favours the formation of glauconite, but that sufficient organic material is necessary to create local reducing conditions. In a review, McRae (1972) concluded that the presence of organic matter is not essential, and that an Eh that is slightly reducing or slightly oxidising (sometimes a reducing micro-environment exists within a macro-oxidising environment) is conducive for glauconite formation. A pH that is slightly alkaline (pH 7-8) is believed to be favourable for the formation of glauconite (McRae 1972; Odin 1988) while temperatures ranging between 15° and 20°C are also believed to be favourable (McRae, 1972).

Several theories regarding the process of glauconitization have been postulated through the years ranging from co-precipitation of Mg, Fe, Al and Si gels, to which potassium was attracted, to the alteration of mud. For the purpose of this study the layer lattice theory first described by Burst (1958), and reviewed by McRae (1972), and a mechanism proposed by Odin (1988) will be briefly discussed. According to the layer lattice theory the formation of the mineral glauconite requires a degraded layer silicate lattice, a plentiful supply of iron and potassium ions and a suitable redox potential. The process of glauconitization then involves the absorption of iron and potassium ions by the degraded lattice and the subsequent reduction of the amount of expandable layers, which will lead to the eventual composition and structure

of glauconite. The degraded lattice should have a low lattice charge, as a high lattice charge will lead to the adsorption of potassium and the collapse to a non-expandable lattice. The expandable layers seem to be necessary for the initial adsorption of iron before it diffuses into the octahedral sheet to replace aluminum. Burial of the mineral will stop the glauconitization process to give a low-potassium disordered glauconite mineral. This might explain the higher potassium and iron values of glauconite from older geological epochs where sedimentation rates were slow. The higher potassium values, in older glauconites, can also be due to post-diagenetic potassium gains.

Odin (1988) found glauconitization to be a two-step crystal growth process while studying glauconite pellets from the Gulf of Guinea. According to Odin (1988) the initial mineral in which the glauconite grows usually do not have a 2:1 structure. Odin (1988) proposes that firstly a glauconitic smectite forms from the crystal growth of neoformed minerals by using cations. A ferric, slightly potassic, smectite is the result, and potassium enrichment only occurs in the second stage of the mechanism. The mechanism involves a recrystallization process into a potassium-rich mineral structure of cations gathered in a potassium-poor structure.

Odin and Fullagar (1988) concluded that nearly all components of a sediment may become green, provided that they are in granular form. According to them no mineralogically similar substrate is necessary for glauconitization to occur.

### 3.9 World wide occurrence of glauconite

According to Odin (1988) and Hillier (1995) the distribution of glauconite is mainly concentrated in continental shelf areas (Fig. 10) especially at tropical latitudes, but glauconite is also reported to occur from latitudes 50°S to 65°N as shown by Odin (1988).

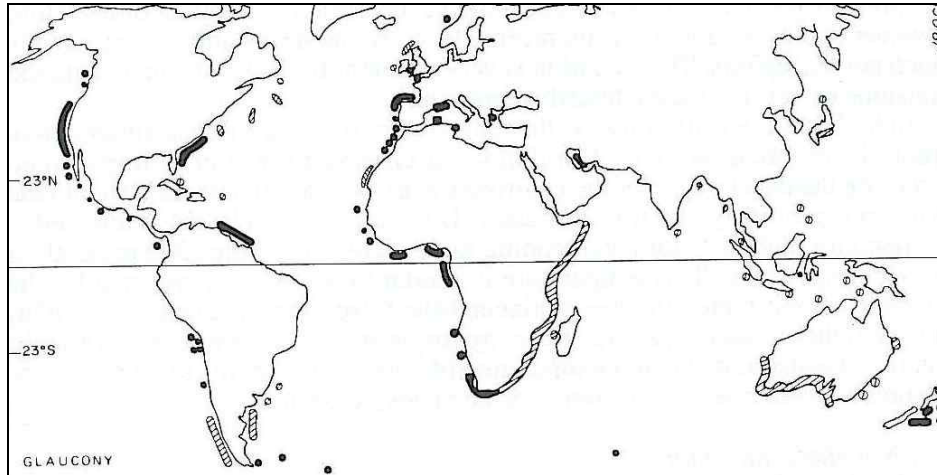


Figure 10. Worldwide occurrences of glauconite on the present-day sea-bottom. After Odin (1988).

### 3.10 Occurrence of glauconite in South Africa

Rich glauconite deposits cover large areas of the continental margin off the south and west coasts (Fig.10) of southern Africa (Birch *et al.* 1976), and apart from this marine glauconite, reports of possible glauconite in pans in South Africa include those by Schmidt (1976), Buhmann *et al.* (1999) and Netterberg (1969). Other reports of glauconite are those associated with the Vryheid Formation in the northern Karoo coal fields (Winter 1985; Cadlle 1995; Hagelskamp 1987 and Barton *et al.* 2004). According to Barton *et al.* (2004), the glauconite is strata bound and the stratigraphic position is site specific, usually in mudstone, siltstone and/or fine-grained sandstone.  $Fe_2O_3$  values of this glauconite, place it, according to Hillier (1995), in a terrestrial glauconite compositional range.

### 3.11 Terrestrial glauconite

Glauconite is traditionally regarded as typical of a marine environment and Millot (1970) rightly said: “This fact belongs to the alphabet of every geologist”. However, some non-marine glauconites are mentioned in the literature and these will be discussed briefly. Millot (1970) mentioned two earlier reports of possible non-marine glauconite by himself, but the formations had mixed characteristics and a marine environment could not be excluded. In Table 2 some reports of terrestrial glauconite with their associated environments and/or origins are listed as reported by Porrenga (1968). Porrenga (1968) concludes that most of these glauconites have compositions that lie between that of illite and glauconite. The environment in which the terrestrial glauconite formed, is in almost all the reports thought to be lagoonal or lacustrine and associations with gypsum are noted in several. Keller (1958)

reported terrestrial glauconite that formed by the alteration of feldspar in volcanic ash within a lacustrine basin environment. Parry and Reeves (1966) and Porrenga (1968) identified glauconitic mica that had structural formulas intermediate between glauconite and illite. The glauconitic mica of Parry and Reeves (1966) was found in recent sediment in one of the Mount Lynn lakes (U.S.A.) from where sepiolite was also later reported (Kossovskaya and Drits 1970). It is now believed that the example described by Porrenga (1968) was in fact reworked glauconite (Hugget and Laenen 1996). Another entry of terrestrial glauconite in the literature is that of Weaver (1975) who mentioned glauconites believed to have formed by the alteration of detrital illite and/or montmorillonite. Kossovskaya and Drits (1970), after reviewing the literature, confirm that continental glauconite differs chemically from marine glauconite in having a lower iron content and that they match the chemistry of ferric illite better. A terrestrial origin is argued for the glauconite studied by Hagelkamp (1987) where biotite is believed to be the precursor mineral while fecal pellets are replaced by glauconite in the Highveld coalfield (Winter 1985).

Table 2. The occurrences and origins of terrestrial glauconite as reported by Porrenga (1968).

Clay	Illite ferrique	Glauconitic mica	Glauconie	Illite ferrifere	Glauconitic mica	Glauconitic illite
Location	Salins (Cantal), France	Uravan, Montrose County, Colorado	St Jacut du Mene, Bretagne, France	Velay, France	Lake Mound, Lynn and Terry Cts, Texas	Aardebrug, Belgium
Age	Oligocene	Late Jurassic	Not specified	Oligocene	Pre-Wisconsin	Lower Oligocene
Formation/member	Zone III	Brushy Basin shale member, Morrison fm	Not specified	Central zone, middle series	Not specified	Kerkom Sand
Occurrence	Thick (100m), horizontally laminated green clay layers. Associated with gypsum	Green interstitial clay in fine-grained clayey sandstone	Green, massive fine-grained clay, Gypsum is present	Thick (15-20m) layers of green clay with thin calcite bands	Green clay layers and streaks beneath present playa. Associated with gypsum	Thin green clay layers and lenses intercalated in sand
Environment/origin	Chemical precipitation in a lagoonal or lacustrine environment	Alteration of montmorillonite in a fluvial or lacustrine environment	Chemical precipitation or alteration of detrital clay in a non-marine continental environment	Alteration of montmorillonite in a lacustrine environment	Alteration of montmorillonite illite or mixed-layers in a lacustrine environment	Alteration of montmorillonite or illite in a lacustrine or lagoonal environment
Author(s)	Jung (1954)	Keller (1958)	Nicolas (1962)	Gabis (1963)	Parry & Reeves (1966)	Porrenga (1967)

#### **4 Laboratory methods and procedures**

Samples were dried in a fan oven at 35°C and split into sub-samples that were analysed at the Council for Geoscience (CGS) in Pretoria by X-ray diffraction (XRD) and X-ray fluorescence spectrometry (XRF). Selected samples were also studied under light and electron microscopes (SEM). Two water samples were submitted for chemical analysis by Inductively Coupled Plasma Mass Spectrometry (ICP-MS) whereas anion species were determined by Ion Chromatography (IC), while the pH was determined in the laboratory using a digital pH meter and preparing a paste with distilled water. Selected samples were sent to the McAuley Institute in Aberdeen, Scotland for Fourier Transform Infrared Spectrometry (FTIR) and three samples were sent for thermoluminescence (TL) age measurements to the Quaternary TL Survey, UK.

##### **4.1 X-Ray Diffraction (XRD)**

Whole rock and clay fraction analyses were performed to determine mineral assemblages. The samples required no crushing prior to milling it for whole rock analysis.

###### *4.1.1 Sample preparation*

###### **Whole rock XRD powder mounts**

Samples were milled into a fine-grained powder of around 10µm before an aliquot of each sample was pressed into an aluminum frame against a rough filter paper, to minimise preferred orientation.

###### **Clay fraction preparations**

The <2 micron fractions were concentrated using the following procedure: ~50g of the crushed sample was dispersed in ~ 300ml water and further disaggregated for ~1min in an ultrasonic bath. After allowing the sediment to settle according to size under gravity for at least half an hour, the top layer, <4µm suspension, was extracted with a pipette, centrifuged and an orientated clay smear was prepared from the residue. Because of the sensitivity of glauconite towards acids (Bentor and Kastner 1965) no carbonates were removed.

###### **Chemical treatment of clay fractions**

Mg saturation was performed on the auger samples from Koi Pan and Brak Pan. The method described by Moore and Reynolds (1997) was followed where the samples were washed with a 1M magnesium chloride solution. All the clay preparations were exposed overnight to ethylene glycol vapour at 60°C, following the procedure described by Moore and Reynolds (1997). Glycerol solvation was performed in a similar manner as the ethylene glycol

solvation, but heated to 80°C and only the samples that were saturated with Mg were exposed.

#### Heat treatment

Clay preparations were heated in a muffle furnace at 550°C for 45 minutes to achieve dehydroxylation.

#### 4.1.2 Instrumentation

Samples were analysed with a Siemens D500 X-ray Diffractometer goniometer equipped with a Cu tube, variable slit and secondary graphite monochromator. The random powder and clay preparations were scanned from 2 to 65° and 2 to 28° 2 $\theta$  Cu $_{K\alpha}$  respectively at a speed of 0.02°/2 $\theta$  step size with a 1 second counting time with generator settings of 35kV and 25mA. The XRD traces were evaluated qualitatively with SIEMENS DIFFRAC<sup>Plus</sup> software and the evaluation program (EVA) allowed matching of the peaks with the PDF-2 Database. Semiquantitative phase estimates of the whole rock powder mounts were based on peak-height percentages as described by Brime (1985).

#### 4.2 Fourier Transform Infrared (FTIR)

The clay fractions of selected samples were concentrated at the CGS prior to submission for mineralogical analysis by FTIR at the MacAuley Institute, Aberdeen, Scotland with Dr. Jean Robertson as the analyst. The glauconite reference material GLO was simultaneously submitted for comparison.

#### 4.2.1 Instrumentation

Spectra from the vertical profile samples collected from Koi Pan, Brak Pan and Gammateep Pan were recorded between 4000 and 400cm<sup>-1</sup> on a Bruker Vertex 70 FTIR spectrometer using a DuraSamplIR DATR (Diamond Attenuated Total Reflectance) accessory with a KRS-5 duradisk. The remainder of the samples were recorded on a Nicolet Magna-IR 550 FTIR spectrometer fitted with a potassium bromide beam splitter and a deutroglycine sulphate detector. Spectra were acquired at 4cm<sup>-1</sup> resolution by the co-addition of 200 scans over the range 4000 to 350cm<sup>-1</sup>.

#### 4.3 Petrography and Scanning Electron Microscopy (SEM)

Bulk samples from selected pans were studied with a light and electron microscope (SEM) at the CGS, Pretoria in an attempt to visualise any clay minerals that may be present. In addition the variation of elemental composition within the fine-grained matrices of samples was studied using X-ray elemental mapping.

#### *4.3.1 Sample preparation*

Samples were impregnated with resin, mounted onto glass slides and polished for studying with transmitted light microscopy prior to carbon coating them for SEM work.

#### *4.3.2 Instrumentation*

Samples were analysed with a Scanning Electron Microscope (SEM) – Leica 440 Stereoscan equipped with INCA (OXFORD) Energy Dispersive System (EDS). Backscattered electron imaging, energy dispersive X-ray analysis and X-ray mapping were performed with the probe current set at 2nA, the accelerating voltage set at 20kV and at counting times of 60s. The default reference standards as supplied by Oxford's INCA software were used to acquire standardless analyses.

#### 4.4 X-Ray Fluorescence (XRF)

Bulk samples were submitted for major and trace element analysis at the CGS, Pretoria.

#### *4.4.1 Sample preparation*

For major element analysis the milled sample (<75µm) was roasted for at least 3 hours at 1000°C to oxidise Fe<sup>2+</sup> and S and to determine the loss on ignition (L.O.I.). Glass disks were prepared by fusing 1.0g roasted sample and 9.0g flux consisting of 34% LiBO<sub>2</sub> and 66% Li<sub>2</sub>B<sub>4</sub>O<sub>7</sub> at 1050°C. For trace elements analysis ~12.0 g of milled material (<75µm) was mixed with 3.0g Hoechst wax, poured into an aluminum backing and pressed at 25 tons with a hydraulic press to produce a powder briquette.

#### *4.4.2 Instrumentation*

The major and trace elements were analysed on a PANalytical Axios X-ray fluorescence spectrometer equipped with a 4kW Rh tube.

#### 4.5 Inductively Coupled Plasma Mass Spectrometry (ICP-MS) and Ion Chromatography (IC)

Two water samples collected at Sout Pan and Gammateep Pan were submitted for chemical analysis at the CGS, Pretoria.

#### *4.5.1 Analytical procedure*

##### ICP-MS

Ultra-pure water (18.2MΩ) was used in the preparation of standard solutions and dilution of samples. Analytical grade nitric acid (HNO<sub>3</sub>) was used to stabilize the elements in solution.

An aliquot of sample was diluted in 50ml polypropylene volumetric flasks with 2% HNO<sub>3</sub>.

20ppb indium and 30ppb iridium were added as internal standards. The dilution factor was chosen to prevent the clogging of the sample introduction system by high salt concentrations, to prevent the possible saturation of the instrument's detector and to ensure that elements were measured close to the calibration range. The calibration standards for quantitative analysis were prepared by using the Merck VI multi-element standard solution. The standards were prepared in 2% (v/v) HNO<sub>3</sub> to match the sample matrix, with 20ppb indium and 30ppb iridium added as internal standards.

IC

Ultra-pure water (18.2MΩ) was used in the preparation of standard solutions and dilution of samples. An aliquot of sample was diluted sufficiently to ensure that the conductivity peak heights fell to within the detection range. The eluent was a carbonate/bicarbonate solution and the regenerant a weak sulphuric acid solution.

#### *4.5.2 Instrumentation*

A Perkin Elmer ELAN® DRC II ICP-MS system, equipped with a Meinhard nebulizer and a Cyclonic quartz spray chamber, was used to determine major and trace elements abundances in the samples while a Dionex QIC analyzer with an automated sampler and a IonPac AG4A guard Column and a IonPac AS4A Analytical Column were used to determine the anion species.

#### 4.8 Thermoluminescence Age Measurements (TL)

Three samples, two from Brak Pan and one from Koi Pan, were submitted for TL age measurements at the Quaternary TL Survey, UK, with Dr Nick Debenham as the analyst.

##### *4.8.1 Analytical procedure*

###### Palaeodose Evaluations

The fine-grained fraction of each sample was selected and dispersed in dilute hydrochloric acid to remove any carbonate minerals present. Sediment grains of between 2µm and 10µm in size were separated from the bulk sample according to their settling times in water. The grains were washed in water, methanol and acetone, before being deposited from suspension in acetone onto aluminum discs. In order to maximise the most readily bleached TL signal with respect to other emissions, a narrow-band temperature selection was made at 310°C (the lowest temperature consistent with thermal stability) and ultra-violet wavelengths were selected with a Schott UG11 filter. The discs were normalised to second glow readouts

following a standard beta radiation dose.

The sample discs were exposed to daylight for several days to remove the bleachable TL signal. This reduced the TL intensity to between 14% and 18% of the original natural TL at the temperature of 310°C. The bleached discs were then irradiated with various doses of beta or alpha radiation in order to regenerate different intensities of TL emissions. By measuring these discs, the growth curves of regenerated TL intensity *versus* radiation dose could be determined. Natural Regeneration Doses (NRDs) were evaluated where the growth curves intersected the natural TL intensity.

#### Dose-Rate Assessments

Alpha dose-rates were measured by alpha counting the sediment grains, while beta dose-rates were assessed by alpha counting and potassium analysis of the finely crushed sediment.

Gamma radiation has a maximum range in sediments of 30cm, so that the gamma dose-rate to the TL sample depends on a weighted average concentration of gamma-emitting nuclides within a radius of this length. In addition to each TL sample, two further sediment samples were collected at locations close to the TL sample. Finely crushed portions of these samples were examined by alpha counting and potassium analysis. The results showed that radioactivity levels within the deposits were homogeneous. Gamma dose-rates were computed from weighted averages of all the available data. Estimates of the cosmic radiation dose-rates were based on the burial depths of the TL samples. The water content of the sediment influences the dose-rate delivered to the TL sample and so estimated uncertainties in the past water content are included in the error limits of the dose-rates.

#### TL Age Calculations

From the TL measurements, giving the forms of the alpha and beta regeneration growth curves, and from the dose-rate assessments, it is possible to calculate how the latent TL intensity accumulated in the sediments during their burial. The growth of TL intensity is counteracted by decay of the signal which occurs by a non-thermal mechanism with a mean life of approximately 100 ka. The TL age represents the period of time required for the increasing latent TL to match the observed present-day TL intensity. The error limits of the TL dates include random and systematic uncertainties in laboratory measurements and environmental factors, and refer to the 68% confidence level.

## 5 Results

Sample descriptions and locality data are presented in Appendix A with analytical data and illustrations presented in Appendices B to E.

### 5.1 Koi Pan

Green material is not confined to the sediments within the pan but also occurs in older sedimentary horizons, notably those in close proximity to the pan, such as the exposures of sandstone of the Eden Formation preserved in the south-eastern part of Koi Pan (Fig.11). Further away from the pan, on the eastern border, cliffs composed mostly of sandstone of the Eden Formation lack the green colouration (Fig. 12) observed for the outcrop in the pan. Evidence in the field suggests that Koi Pan has developed in an approximate westerly direction, leaving the cliff unaffected by the pan processes.



*Figure 11. Sediment, presumably, from the Eden Formation that outcrops in the south-eastern corner of Koi Pan and shows green colouration.*

Other well defined green sediments are those at pan margins that appear to be ancient pan floor sediments deposited prior to lowering of the local base level. Red Gordonia dune sand overlies these ancient green sediments after the pan expanded in a westerly direction away from the pan margin (Fig. 13).



*Figure 12. Sandstone of the Eden Formation (red) and overlain by white Mokolanen calcrete on the crest of a cliff that is situated on the eastern boarder of Koi Pan.*



*Figure 13. A striking contrast is formed by the green pan sediment on the wall of Koi Pan and red Gordonia dune sand that overlies it. The contact between the pan sediment and the aeolian sand is also very clear from the photograph*

Locality data and descriptions of the samples are tabulated in Appendix A and include the three samples of a vertical profile of the pan sediment taken with a hand held auger (one down to 30cm below the pan surface and the other two down to 60cm and 80cm respectively). The colour of the clayey sediment, that comprised the profile samples, turned progressively greener as the auger proceeded into the pan sediment and became a dark olive green at a

depth of 80cm below the surface. Paste pH values of around 10.4 were obtained throughout the profile.

### 5.1.1 XRD

The whole rock analyses of the three profile samples show virtually the same mineral assemblages: quartz, analcime, plagioclase, K-feldspar, dolomite, calcite, thenardite ( $\text{Na}_2\text{SO}_4$ ), halite, mica and loughlinitite. The concentrations of analcime, dolomite and calcite increased with depth while loughlinitite concentrations decrease, forming the main phase in the shallowest and crust samples. The percentage halite and thenardite are below 8% throughout the profile with the highest percentages occurring in the deepest samples and the lowest concentrations in the pans' crust where halite reaches 4% and no thenardite was detected. Mica concentrations of around 8% are reported at all depths and for the crust samples. The samples taken from the outcrop are dominated by dolomite (up to 75%) and contain the same minerals as the profile samples with the exception of the minerals thenardite and loughlinitite.

The minerals present in the green sediment taken from the pan walls (Fig. 13) were essentially the same as those in the pan sediment but it also lacked thenardite and loughlinitite. Mica was present in all the samples.

The clay fractions of Koi Pan sediment were studied to identify the clay species present and the results are presented in Fig. 14. These diffraction patterns show the results after concentration of the clay minerals and the behaviour of the clays after various treatments. The two main peaks as obtained from the whole rock XRD trace were enhanced and no swelling occurred after treatment with ethylene glycol. To investigate the source of the  $\sim 12.7\text{\AA}$  peak, Mg saturation was performed before exposing the preparation to glycerol vapour in order to determine if vermiculite is present. The peak shifted to  $\sim 12.3\text{\AA}$  after the Mg saturation was performed but showed no reaction to the glycerol solvation. It is therefore suggested that the  $12.7\text{\AA}$  peak belongs to loughlinitite (a Na-sepiolite,  $\text{Na}_2\text{Mg}_3\text{Si}_6\text{O}_{16}\cdot 8\text{H}_2\text{O}$ , first described by Fahey *et al.* (1960) from dolomitic oil shale of the Green River formation, Wyoming where it occurs as a replacement mineral) that exchanged Na for Mg during Mg saturation leading to the collapse of the d-spacing to the familiar  $12.3\text{\AA}$  of sepiolite.

## Koi pan

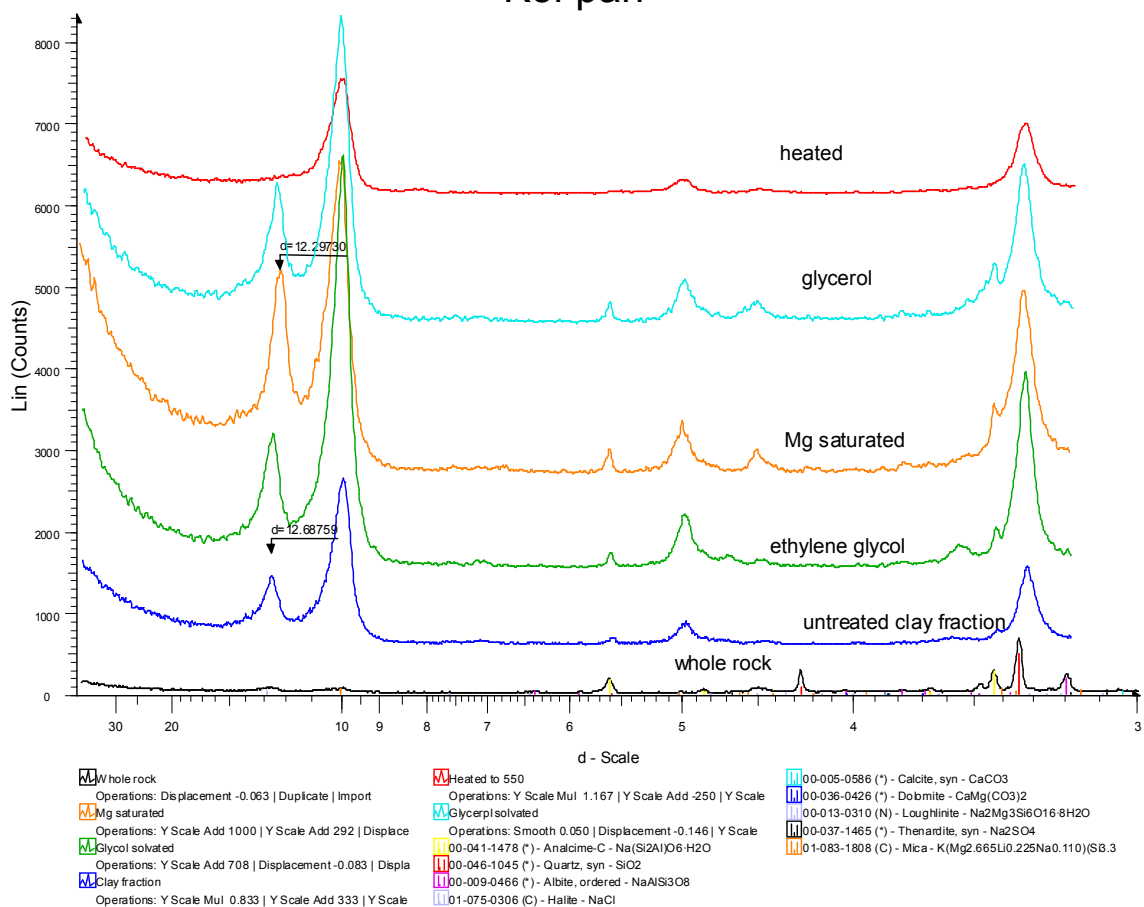


Figure 14. Diffractograms showing the results of various treatments on the clay fraction from Koi Pan sediment.

### 5.1.2 FTIR

The clay fractions of the three profile samples were concentrated and submitted for mineralogical identification by FTIR with special interest in the specific mica. The spectra of the three samples in the OH stretching region are displayed in Fig. 15. The band at  $3558\text{cm}^{-1}$  that corresponds to  $\text{Fe}^{3+}\text{MgOH}$  is present in all the samples, and becomes relatively more intense down the profile, which could be attributed to both glauconite and celadonite. This band is more intense than the bands at  $3602\text{cm}^{-1}$  and  $3534\text{cm}^{-1}$ , the positions of the  $\text{AlMgOH}$  and  $\text{Fe}^{3+}\text{Fe}^{2+}\text{OH}$  stretches for glauconite and celadonite, suggesting a strong Fe/Mg character for the celadonite and/or glauconite. At depth the relative intensity of the absorption bands at  $3602\text{cm}^{-1}$  and  $3534\text{cm}^{-1}$  decreases but simultaneously become slightly more clearly defined, suggesting an increase in the celadonite/glauconite ratio.

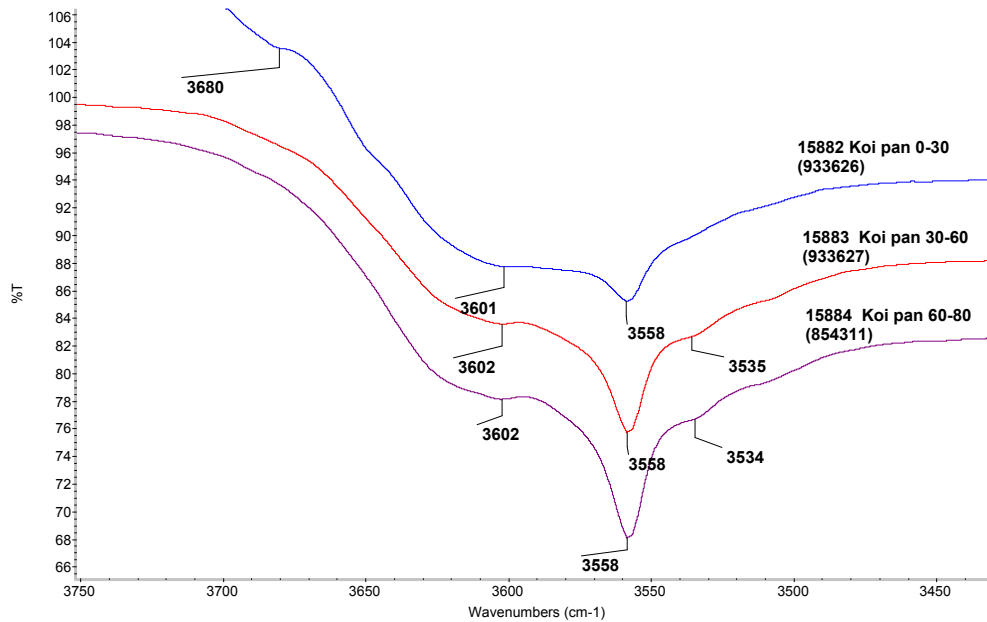


Figure 15. FTIR spectra in the OH stretching region for the Koi Pan profile samples.

Evidence from the FTIR deformation bands appears to back the theory of an increase in the ratio of celadonite to glauconite at depth. The intensity of the band at  $800\text{cm}^{-1}$ , attributed to Fe rich celadonite ( $\text{Fe}^{3+}\text{MgOH}$  deformation), increases down the profile whilst the intensity of the band at  $816\text{cm}^{-1}$  is attributed to glauconite (unresolved doublet due to  $\text{Fe}^{3+}\text{MgOH}$  and  $\text{Fe}^{3+}\text{Fe}^{2+}\text{OH}$ ), and decreases. Another band, more intense in celadonite than in glauconite, at  $\sim 675\text{cm}^{-1}$  is seen in all three samples and appears to become stronger down the profile. The band expected for celadonite at  $838\text{cm}^{-1}$ , which would be due to  $\text{AlMgOH}$ , can not be detected, suggesting a low Al content in the celadonite. Fig. 16 illustrates the bands described in the deformation region. Other minerals identified in the spectra include analcime and a trioctahedral species with a stretching intermediate between talc and sepiolite that appears as a shoulder in the OH stretching region at  $3681\text{cm}^{-1}$ . However, with the available data the exact mineral species could not be identified.

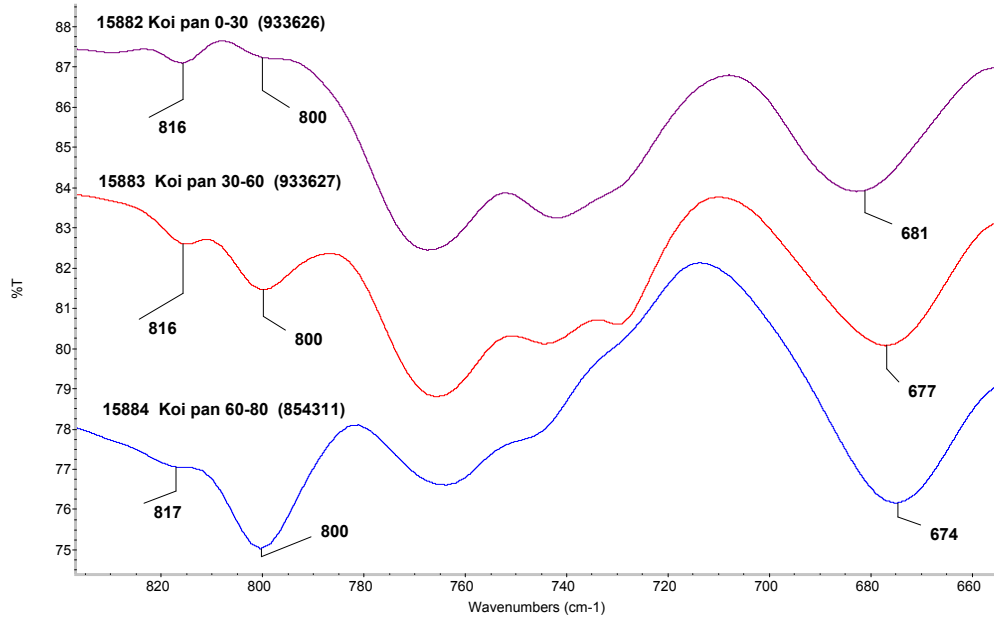
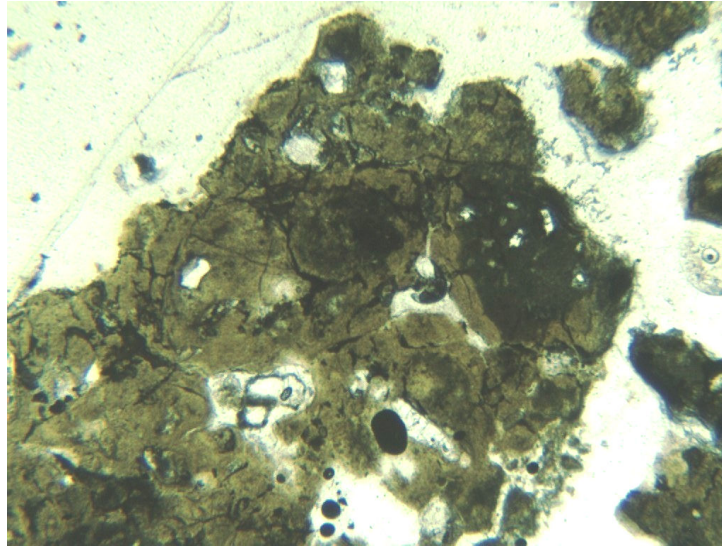


Figure 16. FTIR spectra for the three profile samples from Koi Pan recorded in the OH-deformation region.

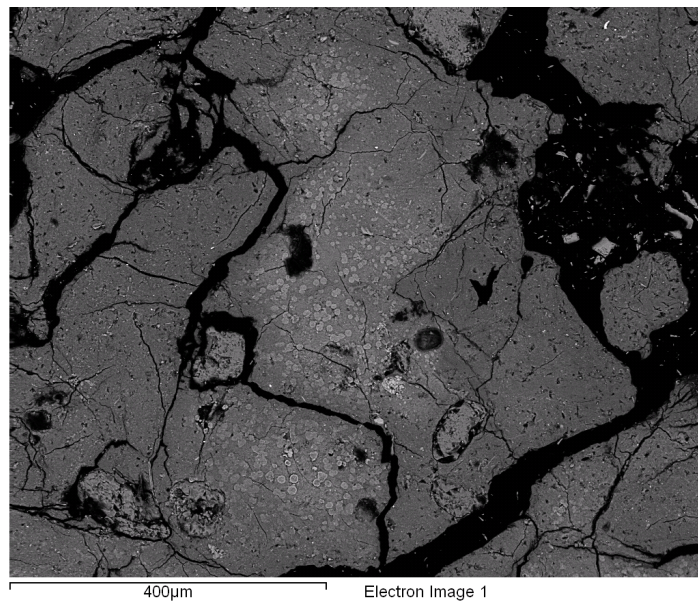
### 5.1.3 Petrography and SEM

Petrographic and electron microscope studies were undertaken on the three profile samples.

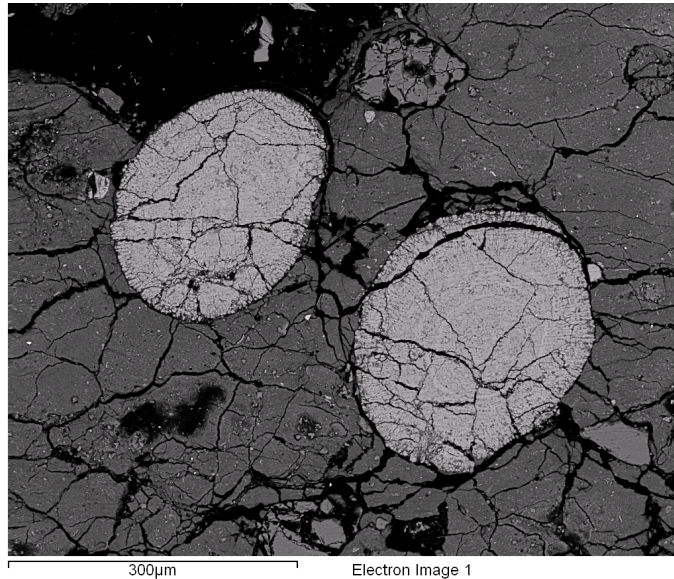
Koi Pan sediment, taken at a depth of 0-30cm below the surface, consists of various fine-grained fragments hosting sub-rounded to angular, sand sized, grains of quartz, K-feldspar, plagioclase and carbonates. Within this brownish-green, fine-grained matrix some greener material is observed that contains finer-grained quartz. In Fig. 17, the pan sediment is shown and in Fig. 18, the BSE image shows patches of what are interpreted as ooids. In Fig. 19, two bigger versions of the ooid structures are shown.



*Figure 17. Photomicrograph of Koi Pan sediment taken at a depth of 0-30cm showing a greenish-brown clayey matrix hosting mineral fragments and darker green material. Plane polarised light. Width of field of view: 2.5mm.*

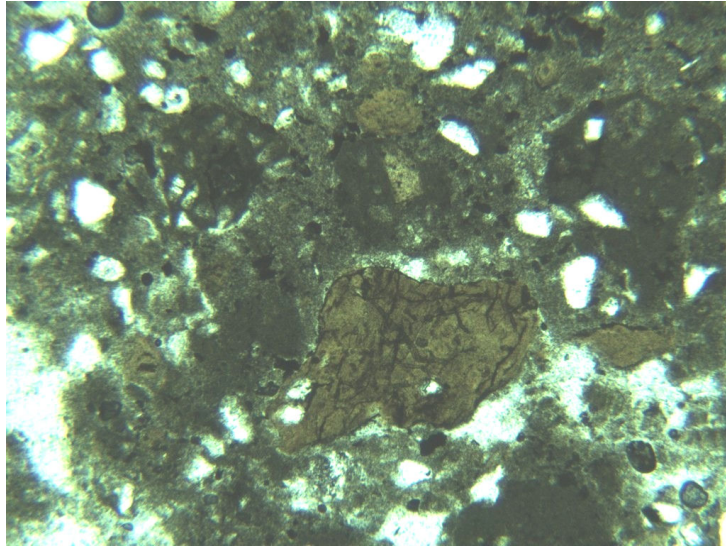


*Figure 18. BSE image of the fine-grained matrix of Koi Pan sediment taken at a depth of 0-30cm below the surface showing light patches interpreted as ooids.*

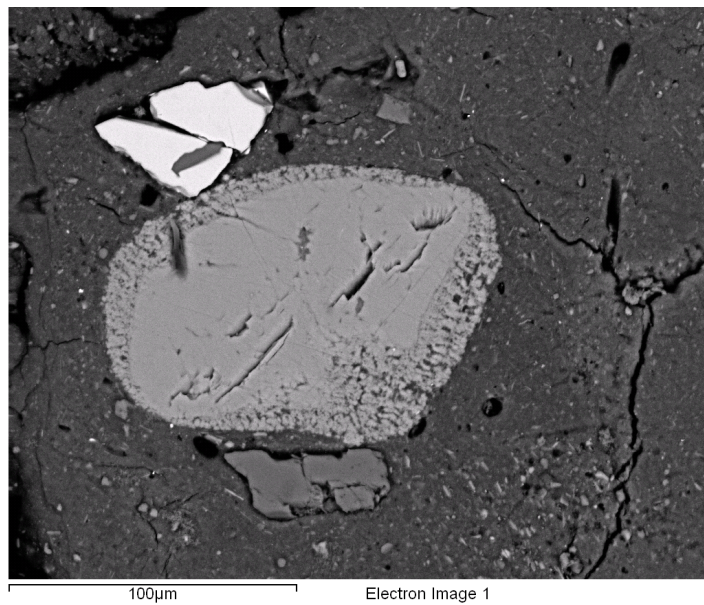


*Figure 19. BSE image showing a fine-grained matrix and ooids showing concentric growth circles and on the outer margin of the nodules some radial growth crystals.*

The sample of Koi Pan 30-60cm consists of the same minerals as found in the Koi Pan 30-60cm sample, but the matrix appears to be olive green in colour (Fig. 20). A number of denser, darker green nodules also containing the mentioned mineral grains occur scattered throughout the thin section. Some of these nodules appear to have clayey rims and considering the clay minerals reported by XRD analysis it is believed to be loughlinite and/or mica rims. Numerous irregular shaped brown clayey materials occur as patches seemingly pseudomorphous after an unknown precursor, throughout the section. A single ooid, with a quartz nucleus, was observed under the light microscope while more were observed with the SEM where EDS analyses showed it to have a calcite composition (Fig. 21).

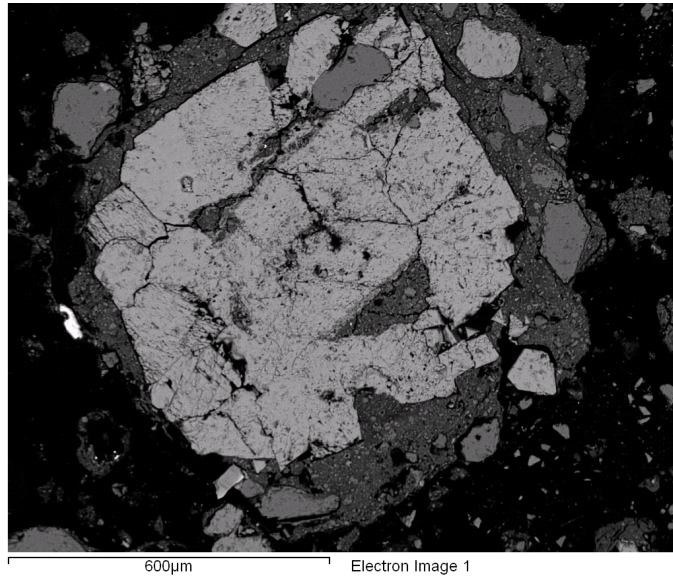


*Figure 20. Photomicrograph of the sample taken at a depth of 30-60cm from Koi Pan showing an olive green matrix and an irregular clayey patch. Plane polarised light. Width of field of view 0.6mm.*



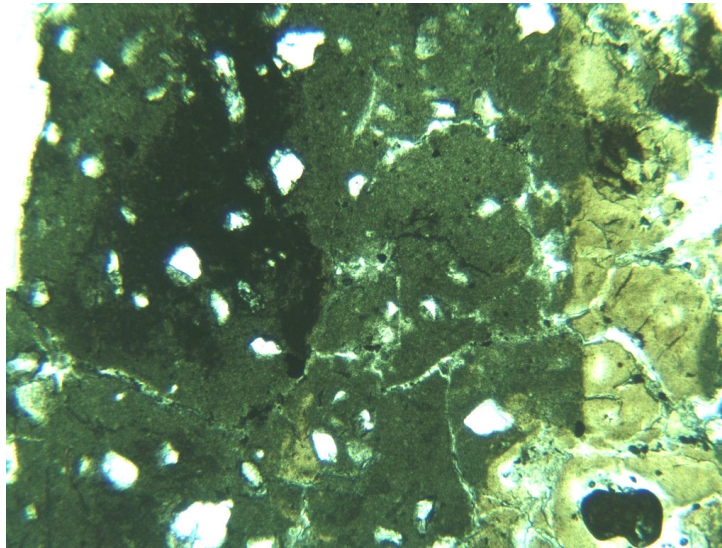
*Figure 21. BSE image of what appears to be a calcitic ooid set in the fine-grained matrix of the sample taken at a depth of 30-60cm from Koi Pan.*

Fig. 22 shows an euhedral calcite crystal (~600µm in diameter) with smaller euhedral dolomite crystals (~10µm in diameter) all set in the fine-grained matrix.



*Figure 22. BSE image of calcite crystals set in a fine-grained matrix in the sample taken at a depth of 30-60cm below the surface of Koi Pan.*

The Koi Pan 60-80cm thin section (Fig. 23) is dominated by numerous fragments of a fine-grained olive green matrix hosting the same mineral fragments as seen in Koi Pan 0-30cm and Koi Pan 30-60cm. The matrix locally appears darker green and finer-grained. Brown clayey patches occur within the fine-grained matrix.



*Figure 23. Photomicrograph of an auger sample taken at a depth of 60-80cm from Koi Pan showing an olive green matrix with a darker green patch to the left and some light brown clay to the right. Plane polarised light. Width of field of view 2.5mm.*

In Fig. 23 the contact between the green matrix and brown coloured clays appears quite sharp, but in other cases the two clay minerals appear more interwoven. Fig. 24 shows calcite crystals set in a matrix hosting various fine-grained minerals with patches of even finer-grained material visible in the bottom left corner. Elemental mapping of the same area showed differences in the matrix (Fig. 25). Grain size (especially visible for calcite and dolomite) appeared to be the main distinguishing feature, but the finer-grained area also seemed to have a higher sulphur content that probably belongs to thenardite.

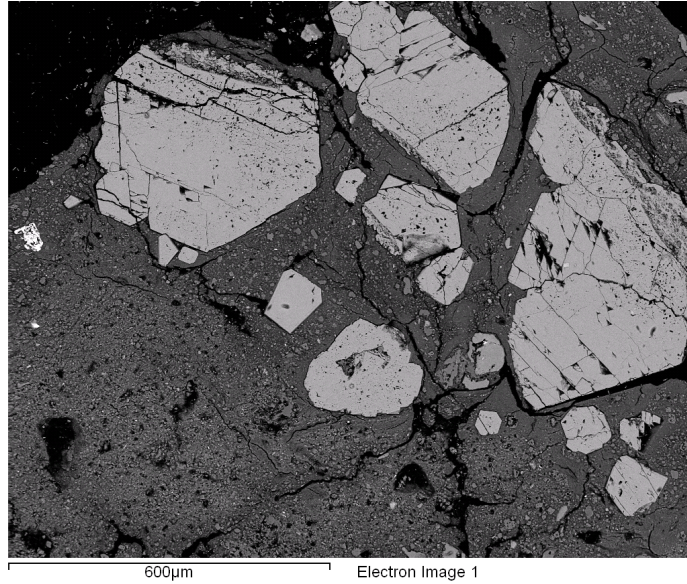


*Figure 24. BSE image of calcite crystals set in a fine-grained matrix and in the bottom left corner some finer-grained material as observed in the Koi Pan 60-80cm sample.*

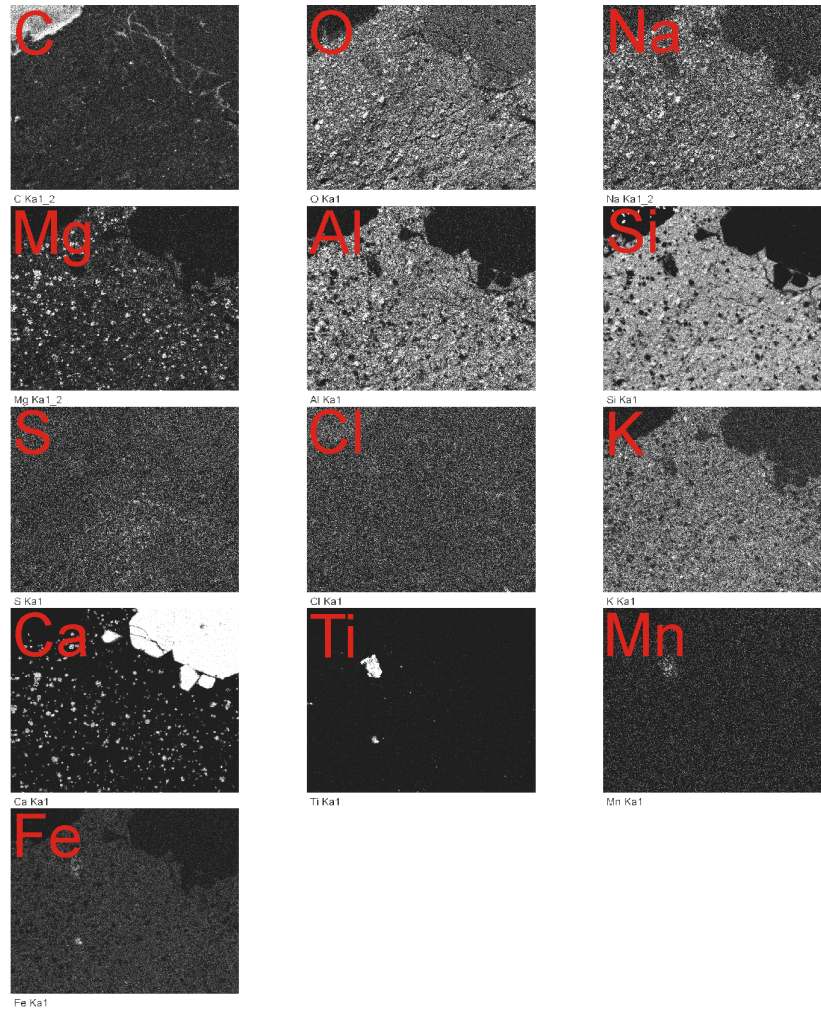
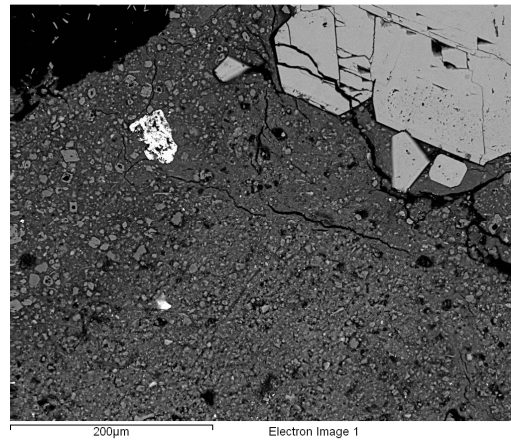
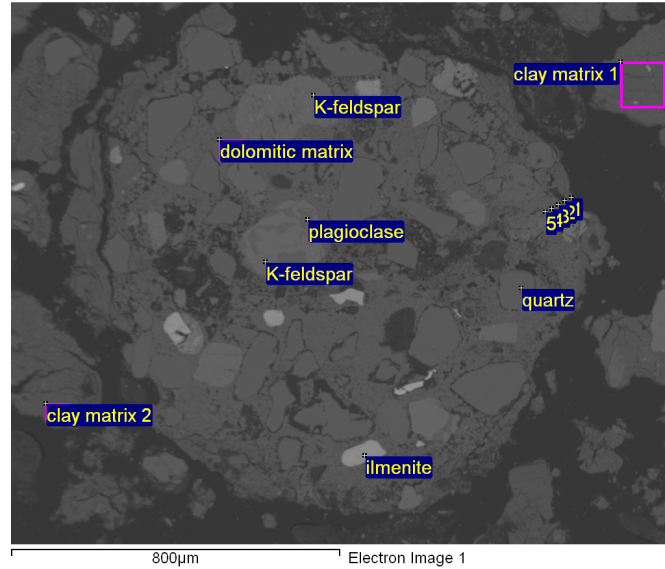


Figure 25. X-ray elemental maps of an area in Koi Pan 60-80cm sediment showing variations in the matrix.

In Fig. 26, an aggregate of minerals is shown as observed in the sediments of Koi Pan. Closer inspection reveals a dolomitic matrix rather than the usual clayey matrix. The aggregate is coated by the previously identified fine-grained matrix composed of Si, Al, Fe, Mg, K, Na and Ti.



*Figure 26. BSE image of an aggregate of minerals as observed in the pan sediment of Koi Pan.*

At high magnification (Fig. 27) the aggregate shows an area in which the dolomitic matrix is in contact with the common fine-grained matrix. Elemental mapping of this area revealed that the iron and the potassium concentrations, that form part of the clayey matrix, seem to concentrate at the contact with the dolomitic matrix, while to a lesser extent the magnesium concentration appears to be lower at the contact. The distribution of aluminum and silica stay unchanged in the clayey matrix.

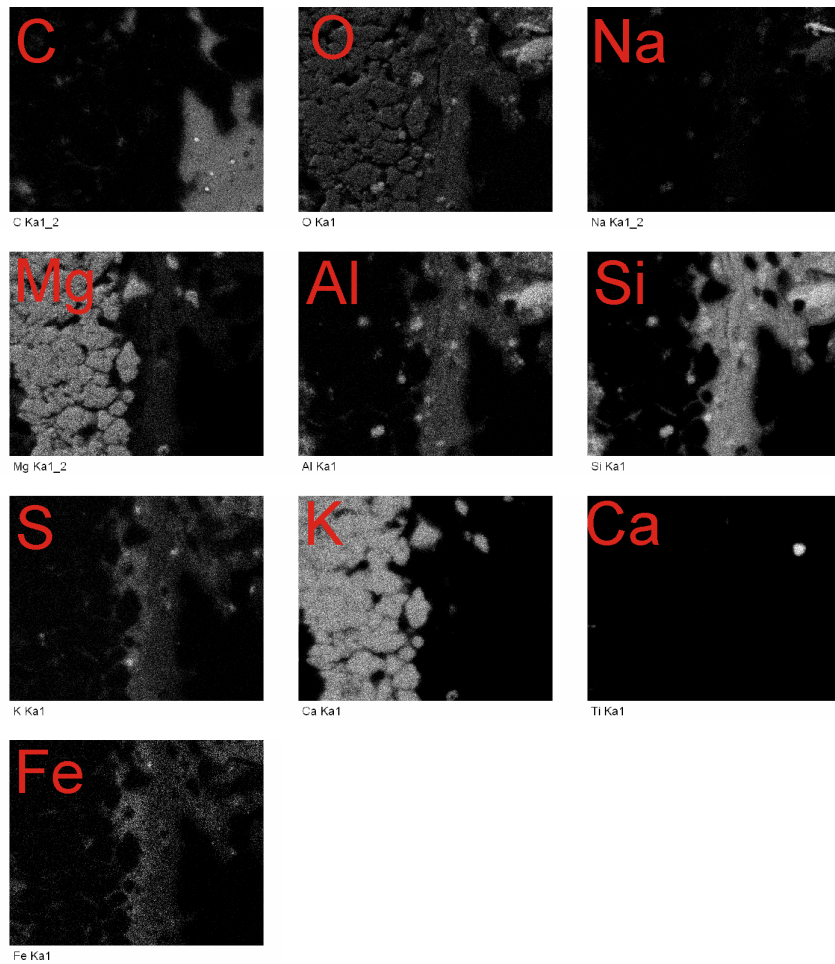
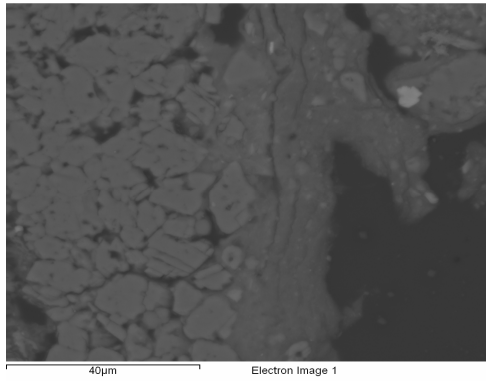


*Figure 27. X-ray elemental maps of the contact between a dolomitic and fine-grained matrix as observed in the sediment of Koi Pan.*

#### *5.1.4 XRF*

The major element analyses (Appendix D), of the three profile samples, shows little variation and no clear trends can be linked to the colour change at depth. SiO<sub>2</sub> values are dominant and range between 54 and 61%. Total Fe values range between 5 and 6% and are the highest compared to the other pans in the study area. K<sub>2</sub>O values stay below 4 %. The relationships between the major elements are illustrated in Appendix D, Fig. D1. The Koi Pan sediment shows positive correlations between Al<sub>2</sub>O<sub>3</sub>, Fe<sub>2</sub>O<sub>3</sub>, K<sub>2</sub>O and Na<sub>2</sub>O while SiO<sub>2</sub> shows no clear correlation with the other elements. MgO and Fe<sub>2</sub>O<sub>3</sub> appear to have a relationship while CaO does not show any correlation with the other elements. Trace element analysis indicated that S occurs in concentrations of between 1.13 and 0.51%. The only other trace elements that occur in amounts higher than 100ppm are: Sr, V, Br, Cr and Ba.

#### *5.1.5 TL age measurements*

The TL age of the Koi Pan sample taken at 120cm below the surface is presented in Table 3. The data refer to the most recent exposure to daylight of the fine-grained component of the sediment while it was transported in a dispersed state. The sample collected in Koi Pan at a depth of 120cm below the surface yielded an age of between 37 and 48ka.

#### *5.2 Gai Gai Pan*

Five vertical profile samples were collected with a hand held auger down to 120cm below the pans' surface and appeared much sandier with no colour change compared to the samples from Koi Pan. The Gai Gai Pan sediments also lack a definite crust in contrast to Koi Pan. Paste pH values of around 10.4 are obtained for the sediments. A conglomerate rock (grit) and sandstone (Fig. 28) were used to construct a dam wall in the pan and these were also sampled and analysed.

Gai Gai Pan (Fig. 29) is used by the owner to accumulate water for sheep, and even though the vertical profile samples were collected at a point away from the recently disturbed soil the possibility that the sediment was contaminated at some point in time must be considered.



*Figure 28. Sandstone from Gai Gai Pan showing a red core with a green alteration rim around the outer margin.*



*Figure 29. Disturbed sediment in Gai Gai Pan. The green colour of the pan sediment forms a contrast with the red dune sand.*

### *5.2.1 XRD*

Generally the same mineral assemblages, as found in the nearby Koi Pan, are encountered in

the Gai Gai Pan sediment with the main differences being in the clay minerals: quartz, K-feldspar, plagioclase, analcime, calcite, dolomite and clay minerals include mica, kaolinite and/or chlorite and smectite. Halite and thenardite concentrations are all below 5%. The quartz concentrations decrease from the deepest sample to the surface and the remainder of the minerals appear to follow an opposite trend. Tests on the clay fraction of the sediment collected at 80-90cm below the surface show mainly mica and some smectite, with very low abundances of either kaolinite or chlorite being present.

The conglomerate (grit) and sandstone samples are dominated by quartz and calcite. Some of the green alteration rim was separated from the red core of the sandstone and analysed. XRD analysis show very little difference apart from a variation in the calcite and dolomite concentrations. The clay fractions of each separate were concentrated and show mica to be the main phase, with the minor amounts of kaolinite or chlorite and smectite in the red separate being absent in the green separate.

### 5.2.2 FTIR

Clay fractions of the sample collected between 80-90cm and from the green alteration zone on the grit were submitted for clay mineral identification by FTIR. The pan sediment from Gai Gai Pan is compared to the spectrum of the glauconite standard GLO (Fig. 30). The most intense band for the Gai Gai Pan sample is at  $3558\text{cm}^{-1}$  and compares well with the bands of the glauconite standard. The very weak band at  $800\text{cm}^{-1}$  observed in the standard is attributed to  $\text{Fe}^{3+}\text{MgOH}$  deformation which arises in the spectrum of Fe-celadonite.

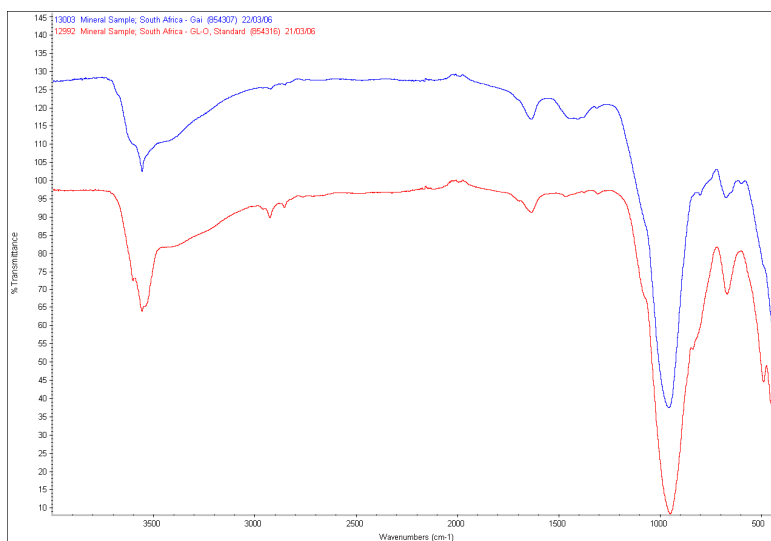
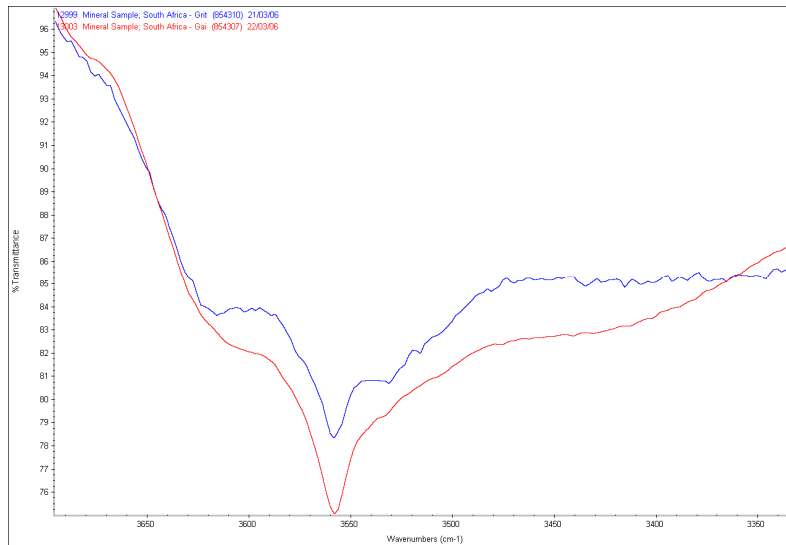


Figure 30. FTIR spectra of the clay fraction from Gai Gai Pan sediment compared to the GLO glauconite standard.

In Fig. 31 the most intense band in the spectrum of the clay fraction from the green alteration zone compares well with the glauconite and/or celadonite reported in Gai Gai Pan sediment.



*Figure 31. FTIR spectra of the clay fraction of sediment sampled in Gai Gai Pan compared to the clay fraction of a green alteration zone seen on grit collected in Gai Gai Pan.*

### *5.2.3 Petrography and SEM*

Petrographic and electron microscope studies were done on the sediment collected at a depth of between 80-90cm, as this sample appeared to be most intense green sample from the whole profile.

The sediment from Gai Gai Pan, as previously shown with XRD, is dominated by quartz grains (Fig. 32) that light and electron microscopic observations show vary in size from ~250 $\mu$ m to less than 1 $\mu$ m and are set in a fine-grained matrix.

In Fig. 33, a BSE image of quartz, feldspar and dolomite grains set in the fine-grained matrix is shown. The quartz grain sizes appear in two distinct populations, one very coarse-grained fraction and another much finer-grained fraction that occur as part of the matrix. Area analysis of the matrix (labelled cm) indicates a chemical composition that comprise of Si, Mg, Al, Fe, K and Na.

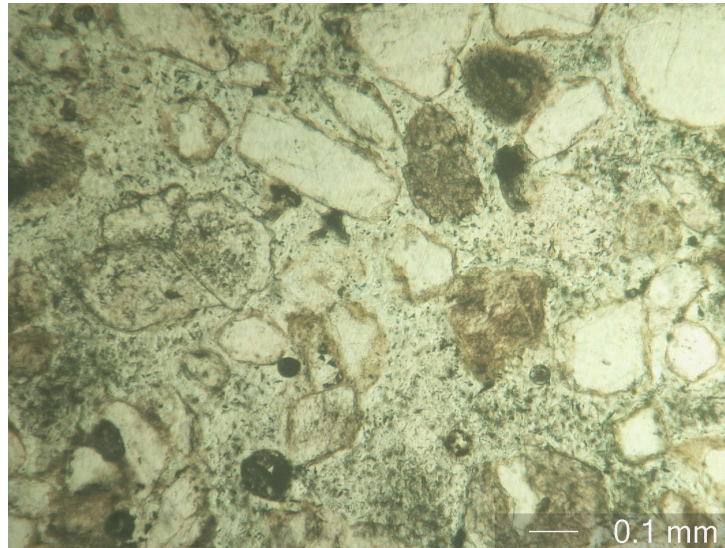


*Figure 32. Photomicrograph of a sediment sample from Gai Gai Pan showing mostly grains of quartz coated by brownish fine-grained material. Plane polarised light. Width of field of view 1.4mm.*

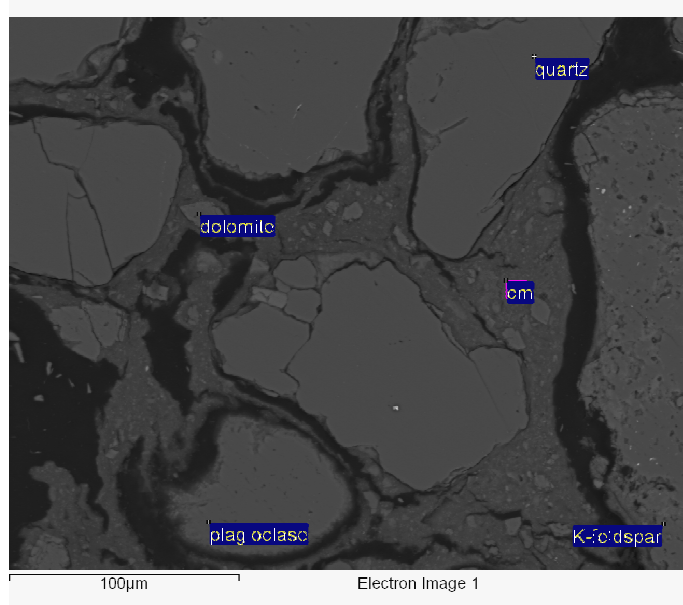


*Figure 33. BSE image of sediment from Gai Gai Pan showing quartz, plagioclase, dolomite and K-feldspar grains hosted by a fine-grained matrix.*

Fig. 34 shows a quartz grain with an unusual fracture filled with the common fine-grained matrix. X-ray element maps of an area showing the contact between the grain and the matrix are shown in Fig. 35. The elemental maps reveal that the Mg concentration is enhanced in the matrix closest to the grain, while the Fe and K concentrations are lower in this region. Away from the quartz grain a region occurs where the Mg concentration is lower than previously detected and the Fe and K reach their highest concentrations before an area is reached where the Al, Si, Fe and K concentrations are lower than before; however, the Mg values appear to stay unchanged. It is assumed that the shielded environment that is created by the shape of the grain might be of importance in the formation of glauconite and/or celadonite.

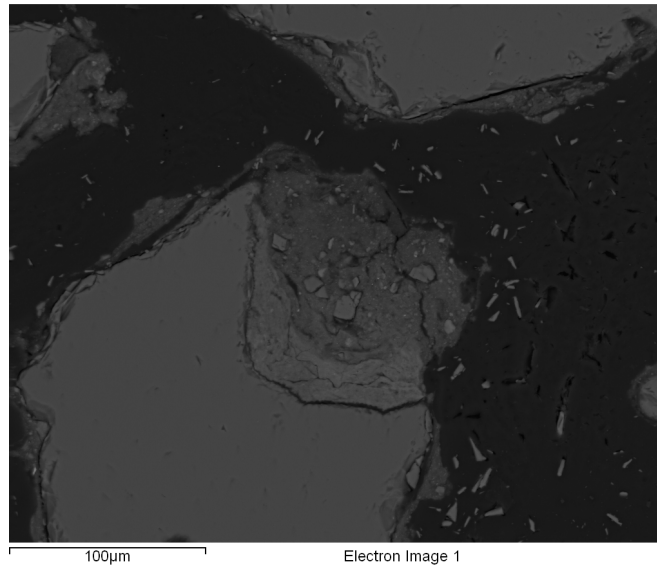


*Figure 34. BSE image of a quartz grain, as seen in Gai Gai Pan, with an unusual fracture that is filled with the fine-grained matrix.*

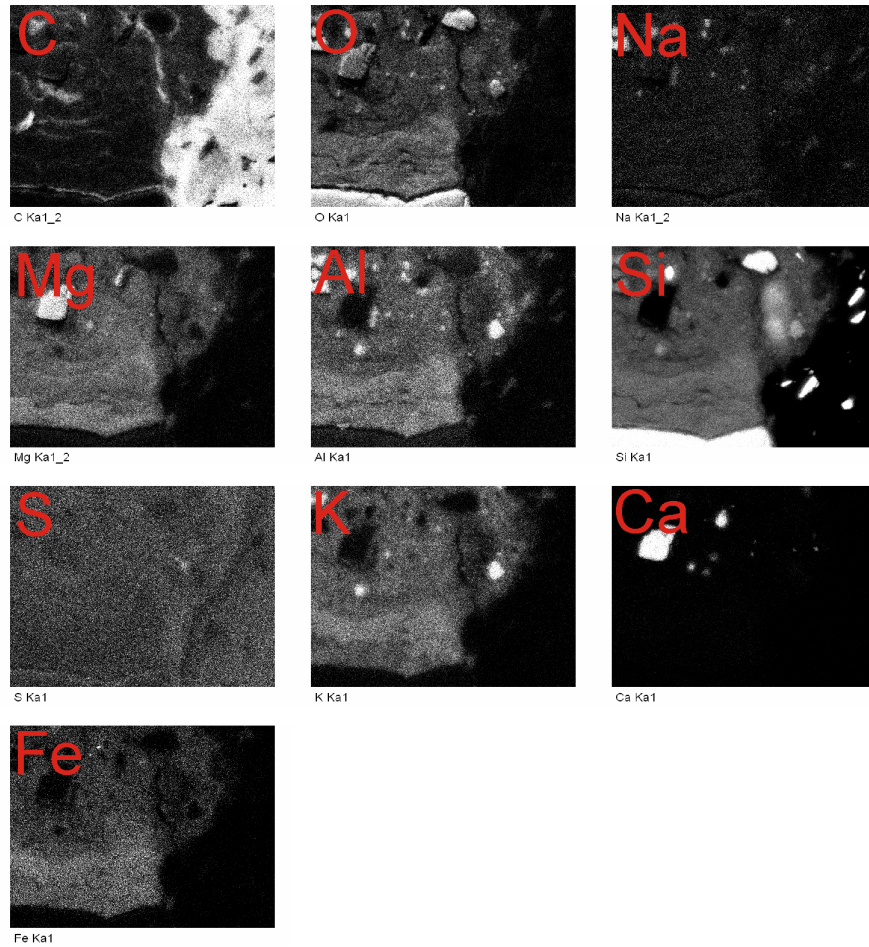
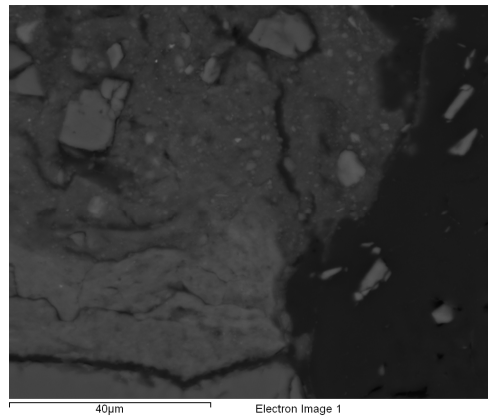


*Figure 35. X-ray element maps showing differences in the matrix occurring in a shielded environment provided by a fractured quartz grain from Gai Gai Pan.*

#### 5.2.4 XRF

The profile samples were submitted for XRF analysis and the results show very high SiO<sub>2</sub> values (Appendix D) that reach up to 86% for the sample collected between 90cm and 120cm below the surface. The other elements appear to concentrate inversely to the SiO<sub>2</sub> content. This is illustrated in correlation curves, of the major elements (Appendix D, Fig. D1) that show Al<sub>2</sub>O<sub>3</sub>, Fe<sub>2</sub>O<sub>3</sub>, K<sub>2</sub>O, MgO and Na<sub>2</sub>O concentrations to roughly correlate with each other while SiO<sub>2</sub> concentrations seem to have an inverse correlation with these elements. CaO concentrations show no strong correlation towards the other elements. Trace elemental analysis shows that S occurs in concentrations of between 0.4%, for the shallowest sample down to 0.17% for the deepest sample. Other trace elements that occur in amounts higher than 100ppm are: Sr, V, Br and Ba.

#### 5.3 Brak Pan

Brak Pan lies untouched by human activities and only the tracks of some animals are testimony of their visits (Fig. 36). Below the salt rich crust, pan sediments have a dark, olive green colour and aggregates, all about 1.5mm in diameter, occur throughout the vertical profile (Fig. 37). Samples were collected down to ~180cm below the surface and were drenched in olive-green fluids that were expelled from an auger hole shown in Fig. 38. pH values of around 10.1 are obtained for the collected sediments by means of the soil-paste method.



*Figure 36. The flat surface of Brak Pan showing salt accumulated in animal tracks and at the back of the photograph the high dunes that form part of the pans' border.*

Crustal material, white salt from the surface of the pan and two vertical profiles of pan

sediment, both down to 1m below the surface, were collected for analysis. Two samples, taken at 110 and 184cm respectively, were collected for TL age determinations.



*Figure 37. Green pan sediment as collected with an auger from Brak Pan. Aggregates lead to the coarse appearance of the sediment.*



*Figure 38. Green fluids expelled from the auger hole during sampling.*

### 5.3.1 XRD

Results for the two vertical profile samples show mineral assemblages that are roughly similar and include: quartz, plagioclase, K-feldspar, analcime, calcite and dolomite (only in the eastern samples). The salts halite and to a lesser extent thenardite occur throughout the profile but seem to reach the highest concentrations in the crust overlaying the pan. Clay minerals include mica (between 3% and 12%) and loughlinite (between 2% and 5%). The concentrated clay fractions of the sediment from different depths show mainly mica and loughlinite with certain samples containing kaolinite or chlorite. Some non-swelling clays (XRD peak around 14Å) were observed in some of the samples. Dune sand seems to be present in higher concentrations in the samples taken towards the eastern side of the pan and probably has a diluting effect on the remainder of minerals.

### 5.3.2 FTIR

Clay fractions of four profile samples collected from Brak Pan (west) were submitted for mineralogical determinations using FTIR. Some aggregates were separated from the matrix material and the clay fractions of both were submitted for analysis and will be discussed after the profile samples. It must be noted that the profile samples represent the clay fractions of the bulk samples (ie. the samples include the aggregates referred to above).

The band at  $3620\text{cm}^{-1}$  (Fig. 39) is generally the strongest OH stretch in the spectra (excluding the Brak Pan 0-20cm sample) and is consistent with illite, but underlying this area may also be a contribution from analcime. A strong, sharp band at  $3558\text{cm}^{-1}$  likely to be from glauconite and/or celadonite is present in all the samples and a contribution to this band from nontronite is a possibility as the band has an OH stretch at  $\sim 3560\text{cm}^{-1}$ . The inflexions at  $3602\text{cm}^{-1}$  (MgAlOH) and  $3534\text{cm}^{-1}$  ( $\text{Fe}^{3+}\text{Fe}^{2+}\text{OH}$ ) in the spectrum of the Brak Pan 40 -70cm are assigned to glauconite and/or celadonite. In comparison to the Koi Pan samples, the celadonite component appears to be much weaker in these profile samples.

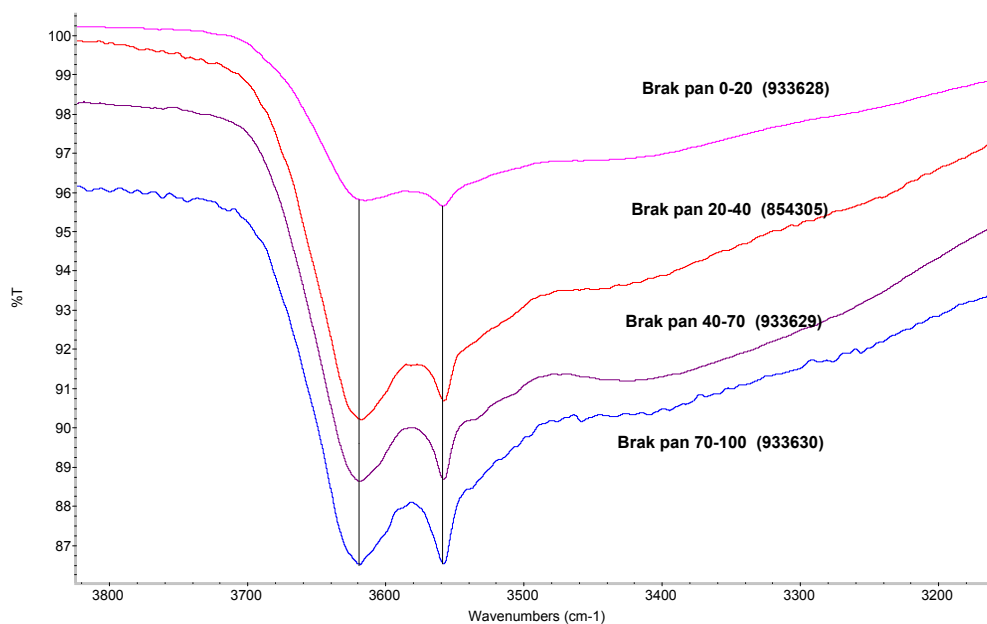


Figure 39. FTIR spectra of the four profile samples from Brak Pan in the OH stretching region

The deformation at  $\sim 830\text{cm}^{-1}$  is considered to be due to illite, although it is close to the position of the celadonite deformation at  $838\text{cm}^{-1}$ . Analcime and quartz bands are observed in all four samples.

The clay fraction of the matrix was separated into a green and a grey portion upon drying and compared to the clay fraction of the aggregates, which also appeared grey when dried. The spectra of the green and grey portions of the matrix both show bands in the OH stretching region that are attributed to illite and celadonite and/or glauconite. In the spectrum of the green sample the stretch at  $3558\text{cm}^{-1}$  (the band that originates from  $\text{MgFeOH}$  in celadonite and/or glauconite) is stronger than the corresponding illite stretch at  $3618\text{cm}^{-1}$  whilst in the grey material it is weaker. Inflections at  $3602\text{cm}^{-1}$  and  $3534\text{cm}^{-1}$  associated with celadonite are visible in the spectrum of the green material, but are not detected in the grey material. The spectrum of the clay fraction of the aggregates show even less celadonite character and more illite character, in the OH stretching region, than the grey clay sample from the matrix.

The amount of quartz varies considerably in these three samples: The clay fraction from the aggregates' spectrum shows a high proportion of quartz, the grey matrix sample' spectrum shows less and the green sample spectrum the least. There are evidence in all three samples for illite (deformation at  $830\text{cm}^{-1}$  and  $\sim 750\text{cm}^{-1}$ ). There are also a celadonite and/or

glaucanite and/or nontronite band at  $817\text{cm}^{-1}$  in the green clay sample and apparently (adding to the quartz band at  $797\text{cm}^{-1}$ ), a band at  $800\text{cm}^{-1}$  which is assigned to celadonite. The band at  $\sim 680\text{cm}^{-1}$  is assigned to celadonite and/or glaucanite as well. The weak  $743/726\text{cm}^{-1}$  doublet in the spectrum of the grey clay sample suggests the presence of analcime. A band at  $649\text{cm}^{-1}$  in the spectra of the grey and green clay samples (stronger in grey than green) can possibly be due to feldspar or chlorite.

### 5.3.3 Petrography and SEM

Because the whole profile appears to be equally green in colour only one sample was chosen and studied with light and electron microscope.

Samples from Brak Pan consist of a fine-grained, yellow-brown matrix containing poorly sorted quartz, feldspar and carbonate grains (Fig. 40). The matrix appears to be rich in clays and contain a number of brownish nodules with a fine-grained matrix typically consisting of finer-grained material. These finer-grained nodules correspond to the aggregates occurring throughout the pan sediment that have illite as the main clay phase. A single ooid with a quartz nucleus was observed.

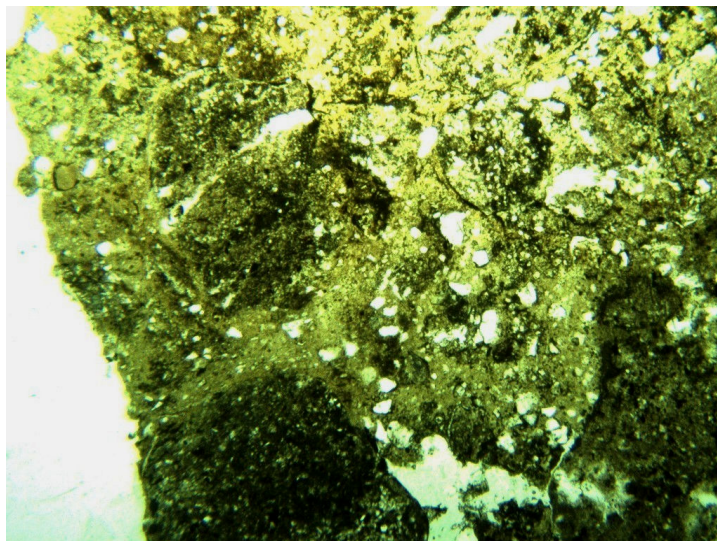


*Figure 40. Photomicrograph of sediment taken from Brak Pan showing a yellow-brown matrix with dark, fine-grained nodules and quartz, feldspar and carbonate grains. Plane polarised light. Width of field of view 2.5mm.*

EDS analyses of the sediment confirmed the minerals identified with XRD and petrography. The domains in the matrix, as observed under the light microscope are shown in Fig. 41 and some chemical differences are illustrated. The darker areas that host a coars-grained fraction

of minerals appear to contain Mg as part of the matrix's composition, but this was absent in the lighter, fine-grained areas (that correspond to the aggregates in the sediment). BSE images of areas in the Mg-rich and the Mg-absent matrices were taken at higher magnification revealing their constituents and matrix chemistry (Fig. 42 and 43).

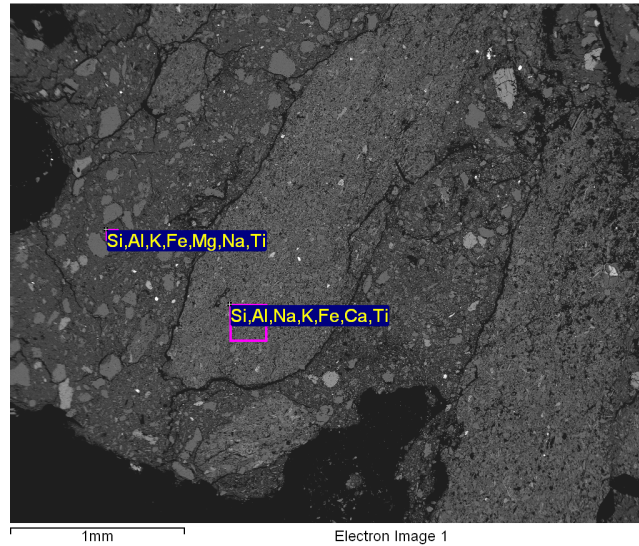


Figure 41. BSE image of sediment from Brak Pan showing domains that differ in their grain size and chemical components.

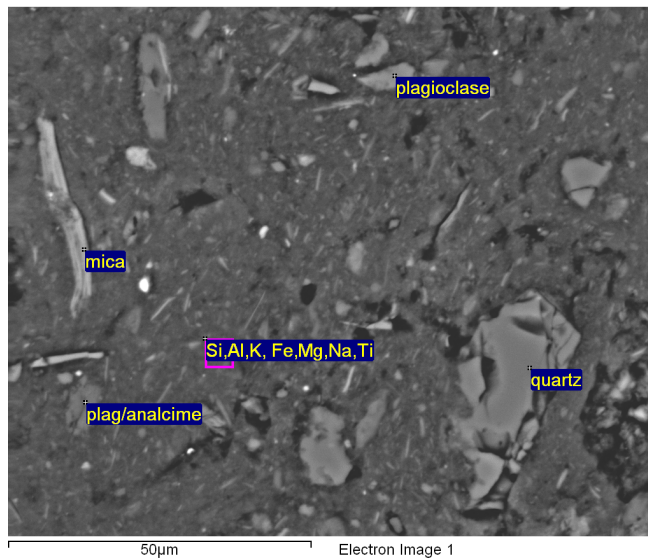


Figure 42. BSE image of an area of the matrix hosting the coarse-grained material showing Mg as part of the chemical make-up.

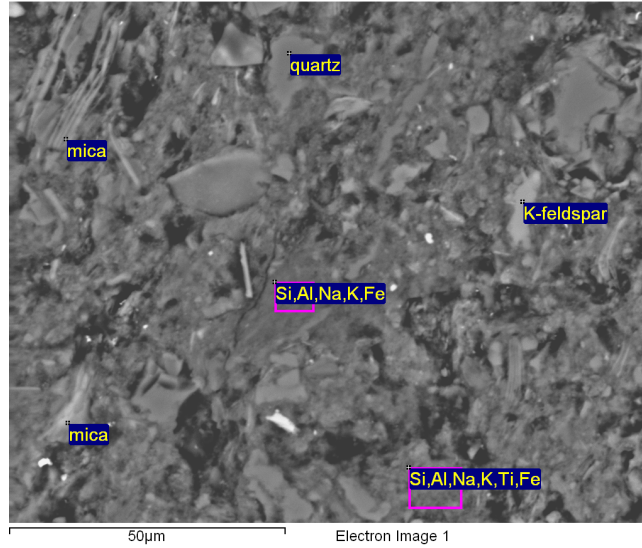
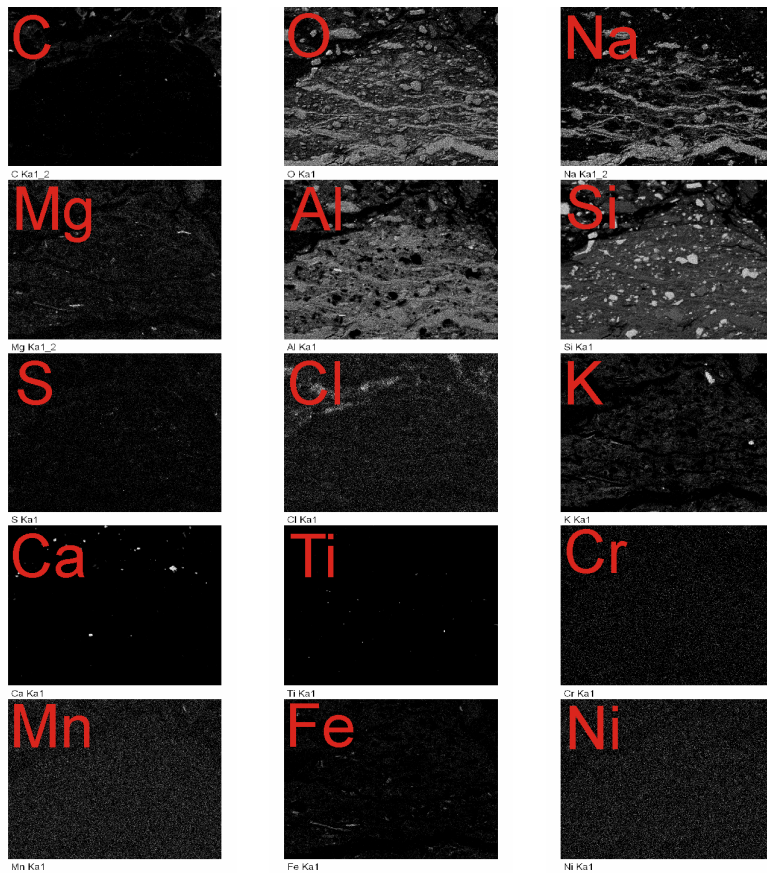
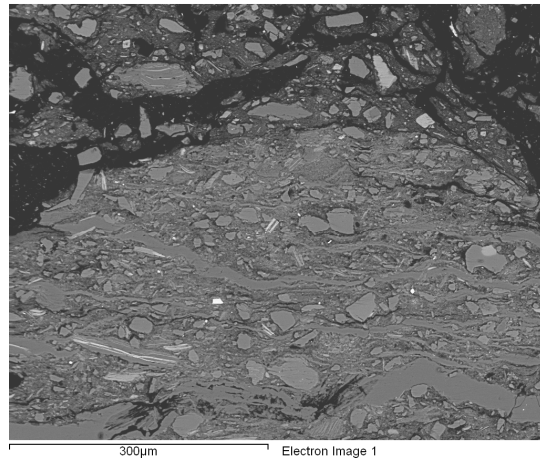


Figure 43. BSE image of an area of the matrix hosting fine-grained minerals.

Apart from the coarse-grained minerals in the one domain (Fig. 42) both the domains contain a fine fraction of generally the same minerals. The appearance of the matrices is also quite different: the matrix of the domain containing the coarse-grained fraction appear much smoother and homogeneous (Fig. 42) than the matrix of the other domain (Fig. 43).

In Fig. 44, elemental maps of a part of fine-grained domain displaying a vein-like texture is shown, with in the top of the image the matrix hosting the coarse-grained material. Judging from the chemical composition and taking the XRD results into account it is suggested that the veins are composed of analcime. In the lower left corner Fe, K and Mg concentrations are high in a line-like feature and it is considered to be mica that runs side by side with the analcime veins. Quartz grains, ~ 50µm in size, occur throughout both matrices and in addition to this much finer-grained quartz was noticed in the matrix at the bottom of the image. In the top matrix, Ca occur as part of discrete mineral fragments and the O, Na, Al and Si concentrations in the matrix appear to be lower, while the Mg concentration seems to be slightly higher.



*Figure 44. X-ray elemental maps of an area showing the different domains in the sediment of Brak Pan. At the top the matrix hosting the coarse-grained minerals and below that the matrix hosting the fine-grained minerals.*

#### 5.3.4 XRF

Bulk chemical data for Brak Pan support the mineralogy as indicated by XRD analysis. Higher SiO<sub>2</sub> values are reported for samples taken from the east of the pan. Correlation curves (Appendix D), show a relationship between Al<sub>2</sub>O<sub>3</sub>, Fe<sub>2</sub>O<sub>3</sub>, K<sub>2</sub>O and Na<sub>2</sub>O, but no clear trend can be deduced for the MgO and CaO concentrations. SiO<sub>2</sub> appears to be concentrating inversely to Fe<sub>2</sub>O<sub>3</sub>, K<sub>2</sub>O and Na<sub>2</sub>O. Trace elemental analysis reveals that S occurs in concentrations of between 1.67%, and 0.52%. Other trace elements that occur in amounts higher than 100ppm were: Sr, V, Br, Zr, Cr and Ba.

#### 5.3.5 TL age measurements

TL ages for the two samples taken in Brak Pan are as follow: older than 110ka at a depth of 110cm below the surface and older than 150ka for the sample taken at 184cm below the surface.

#### 5.4. Opstaan Pan

Large areas of Opstaan Pan have been disturbed by a salt mining company that dug trenches for brine concentration. Samples of salt, sediment from the walls of the trench as shown in Fig. 45, as well as four profile samples, taken down to about 1m below the surface, were collected and analysed. The pan sediment consists of brown and red clayey sand and only below 60cm were some green coloured lumps encountered. pH values of around 9.8 are obtained for the collected sediments (using the soil-paste method).

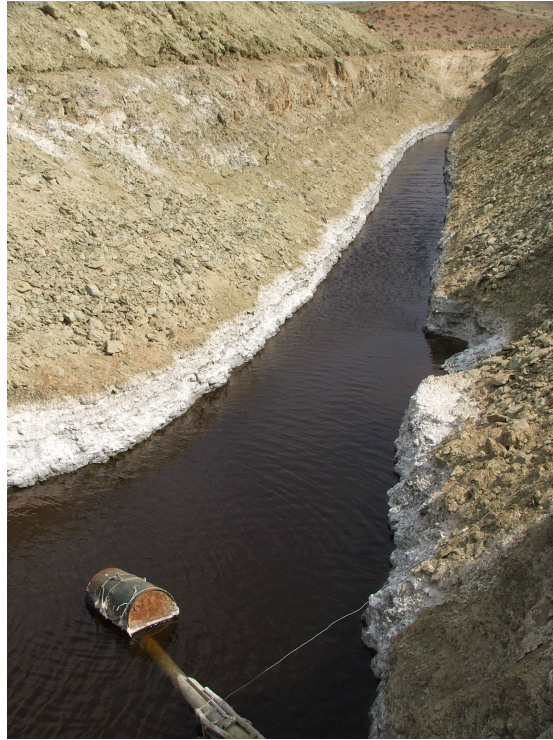


*Figure 45. A trench in Opstaan Pan where brine is being collected.*

#### 5.4.1 XRD

The profile samples are dominated by quartz with other minerals such as plagioclase, K-feldspar, analcime, calcite and to a lesser extent dolomite occurring in lower concentrations. Clay minerals include: mica, kaolinite+/chlorite and smectite. The diffractograms of the concentrated clay fraction of sediment from Opstaan Pan and their subsequent behaviour after treatment are presented in Fig. 46. The swelling of the smectite layers after exposure to ethylene glycol and consequent collapse after heating of the sample while the mica peak stays unaffected are shown. The mineral responsible for a small bump at  $\sim 7.2\text{\AA}$  (already observed in the trace of the whole rock XRD) that can belong to either kaolinite or chlorite remains in question as a broad peak covers both the  $24.9\text{\AA}$  and  $25.1\text{\AA}$  peak positions, thus no definitive distinction could be made. The  $7.2\text{\AA}$  peak remains unaffected after heat treatment but also no enhancement of the (001) chlorite reflection was observed. It was therefore concluded that either kaolinite or chlorite (or both minerals) are present, but in very low concentrations.

The only salt mineral identified in the pan sediment is halite but in the pure salt samples some thenardite is also present. Salt concentrations appear to decrease in a downward direction with the highest values obtained in the samples taken between 60cm and 100cm and corresponding to the position in the profile with the highest reported abundance of mica.

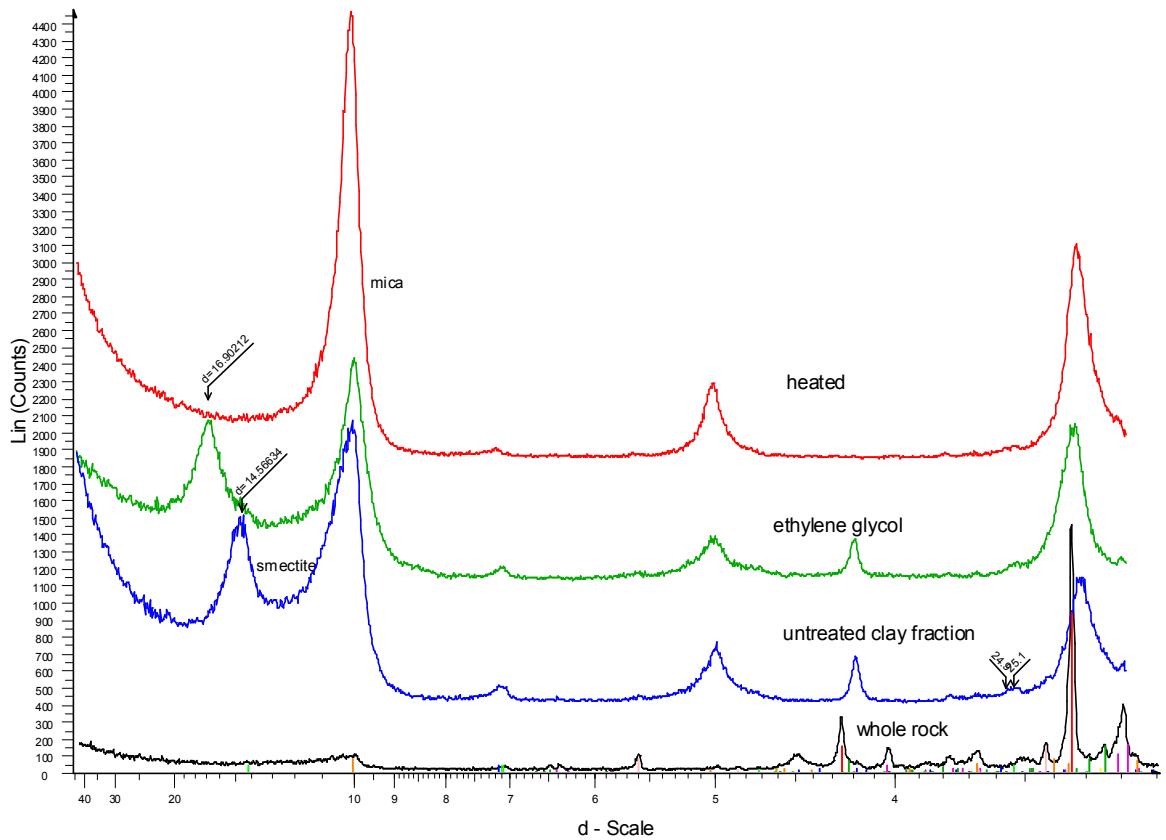


Figure 46. Diffractogram showing the behaviour of clay minerals in Opstaan Pan sediment after various treatments.

#### 5.4.2 FTIR

The clay fraction from Opstaan Pan 85-100cm was submitted for FTIR as this was the only sample that had a green hue. The spectrum shows, in the OH stretching region (Fig. 47), a sharp, distinct band at  $3558\text{cm}^{-1}$  and a shoulder at  $3532\text{cm}^{-1}$  considered to be produced from glauconite and/or celadonite. There is also a broad band at  $3618\text{cm}^{-1}$ , which is the most intense OH stretch, that is attributed to analcime, but could also have a contribution from illite. Analcime also has an absorption band at  $3553\text{cm}^{-1}$  and would be contributing intensity at that wave number.

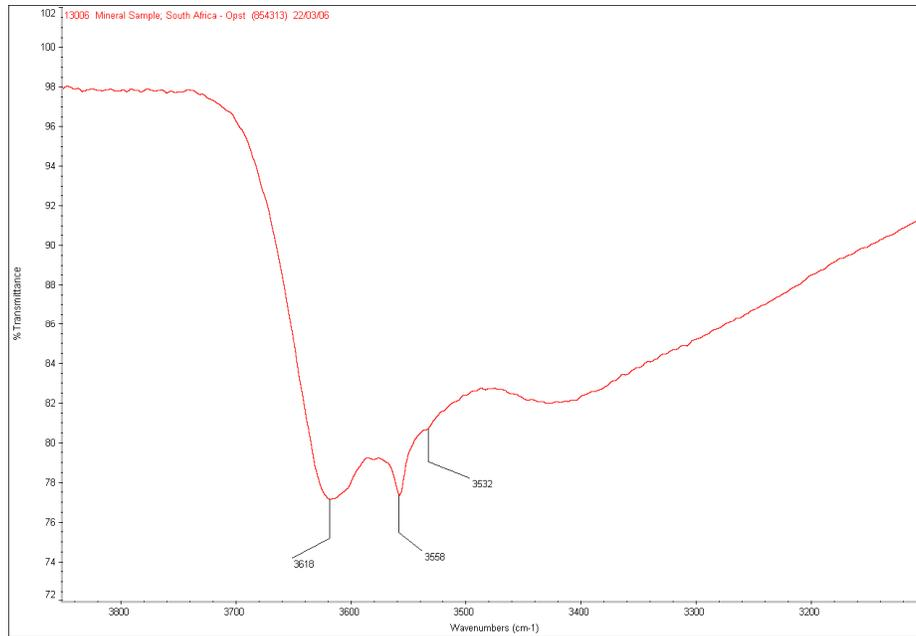


Figure 47. FTIR spectrum of the clay fraction of Opstaan Pan sediment taken at a depth of 85-100cm below the surface.

#### 5.4.3 Petrography and SEM

The sediment from Opstaan Pan appears more brown-red in comparison to the greenish sediment from the other pans, and the overall particle size is much finer-grained (Fig. 48).

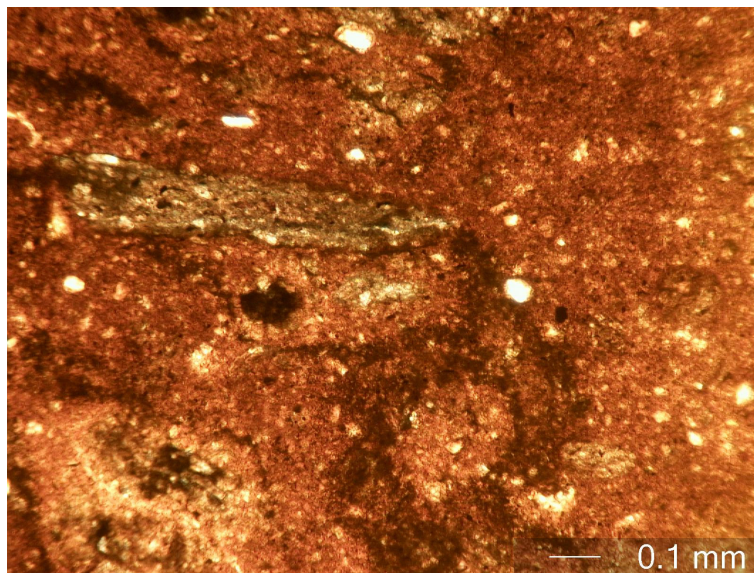


Figure 48. Photomicrograph of pan sediment from Opstaan Pan. Plane polarised light. Width of field of view 1.4mm.

Quartz grains were observed in a matrix that seems to display colour differences varying

between red-brown and yellow-brown. X-ray elemental mapping of the matrix was performed and the results are shown in Fig. 49. The fine-grained nature of the minerals set in the matrix is clear and two domains are recognized on the image. These included a zone of lower Na, Al and Si concentrations that runs between material with higher Si Al and Na concentrations. It also appears that the Fe concentration is slightly higher in the zone where the Na, Al and Si are at lower concentrations. K and Mg concentrations appear to be homogeneous throughout the matrix, while the Ca and Ti appear to be part of discrete minerals.

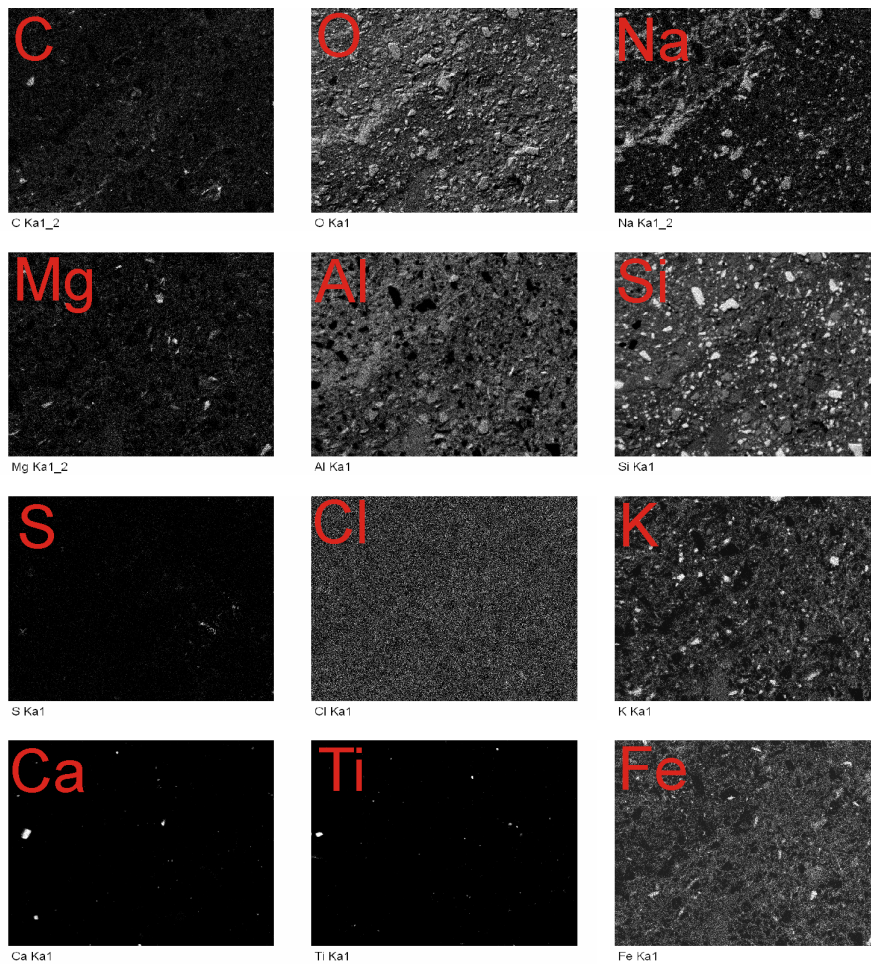
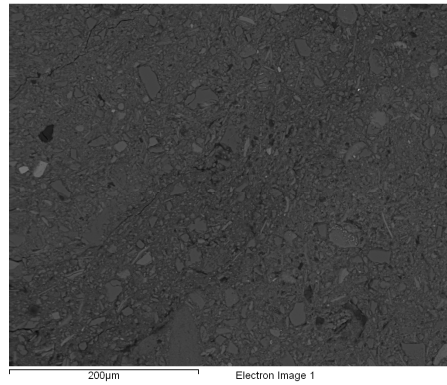


Figure 49. X-ray elemental maps showing chemical differences in the matrix of Opstaan Pan sediment.

#### 5.4.4 XRF

Four samples from the vertical profile were analysed and revealed SiO<sub>2</sub> concentrations that have a negative correlation with the other elements (Appendix D). The correlation curves of the major elements (Appendix D, Fig. D1) suggest that the occurrence of K<sub>2</sub>O, MgO, and Fe<sub>2</sub>O<sub>3</sub>, Na<sub>2</sub>O and CaO are related. SiO<sub>2</sub> appears to be inversely related to the other elements.

Trace elemental analysis shows that S occur in concentrations of between 0.11 and 0.08%. Other trace elements that occur in concentrations higher than 100ppm were: Sr, V, Zr and Ba.

#### 5.5 Sout Pan

Sout Pan is covered by a thick layer of white salt and although a mining company is exploiting these salt reserves, large areas of the crust still lay unaffected (Fig. 50). Two dark green to black profile samples that had a strong sulphurous smell were collected down to 40cm below the pan surface. A sample of the salt-rich crust covering the pan was also taken, as well as the green unconsolidated sediment on the pan wall. pH values of around 9.9 were obtained for the collected sediments by means of the soil-paste method.

Water was collected from the bottom of the auger hole for analysis.



*Figure 50. In the foreground a thick, white salt crust that covers the sediments of Sout Pan and at the back dunes that mark the pans' border.*

#### 5.5.1 XRD

The pan sediment consists mainly of halite with lesser quantities of quartz, plagioclase, analcime, calcite and thenardite. Clay minerals include mica and kaolinite and/or chlorite. The crust samples are dominated by halite (92%) with only minor amounts of quartz and thenardite.

### 5.5.2 ICP-MS and IC

The chemical analysis of the water sample (Appendix E) that collected at the bottom of the auger hole revealed, as expected, very high Na values followed by Ca, K, Al, Mg and Ba. The anion data indicate that the water is dominated by Cl followed by  $\text{SO}_4^{2-}$ .

### 5.6 Gammateep Pan

Gammateep Pan is a very shallow pan in comparison to the pans to the west, with a notably smaller presence of dune sand in its sediment. One sample of the crust covering the pan and four vertical profile samples were collected to about 80cm below the surface using an auger (Fig. 51). Green clayey lumps were hand-picked and submitted for analysis as concentrated green clay. pH values of around 9.0 were determined by using the soil paste method and by applying phenolphthalein. Water was collected from the surface of the pan where it accumulated in a small depression. A green mica schist was collected from a road running adjacent Gammateep Pan and was also submitted for selected analyses.



*Figure 51. Pan sediment taken from Gammateep Pan.*

#### 5.6.1 XRD

The mineral assemblages of the four vertical profile samples consisted of: quartz, plagioclase, K-feldspar, dolomite and calcite. Mica and to a lesser extent illite/smectite interstratification are identified in all samples. No salt minerals are present except in the sample of concentrated green clay which contained halite. The crust is composed mostly of quartz (78%) with the remainder of the minerals being those found in the pan sediment samples and referred to above.

#### 5.6.2 FTIR

The three profile samples as well as the sample of concentrated green material collected at the deepest part of the profile, were submitted for mineralogical determination by FTIR.

The FTIR spectra, in the OH stretching region, of the three profile samples are illustrated in Fig. 52. Down the profile the band at  $3564\text{cm}^{-1}$ , that can be attributed to MgFeOH, becomes

slightly more distinct, which may relate to an increase in the Fe content. However, there could be a contribution from illite hidden under the broad band at  $\sim 3620\text{cm}^{-1}$ . In the deformation region a band at  $800\text{cm}^{-1}$  may be attributed to celadonite or quartz (the band becomes slightly more intense at depth.) There is a suggestion of a very weak band at  $\sim 836\text{cm}^{-1}$  which is approximately where the AlMgOH deformation of a high Al celadonite can be expected, but the deformation of illite also lays close to this wave number.

In the 0-20cm sample there is a weak band stretch at  $3678\text{cm}^{-1}$  close to that seen in Koi Pan samples which corresponds to some trioctahedral species that lie intermediate between talc and sepiolite.

The presence of some other clay or hydrated salt in the sample taken between 40-60cm is suggested by the weak doublet at  $639/614\text{cm}^{-1}$  and most probably represents a sulphate. Carbonate in the form of dolomite is present in all three samples as indicated by the bands at  $878\text{cm}^{-1}$  and  $728\text{cm}^{-1}$  but the concentration decreases down the profile. Quartz appears to increase with depth.

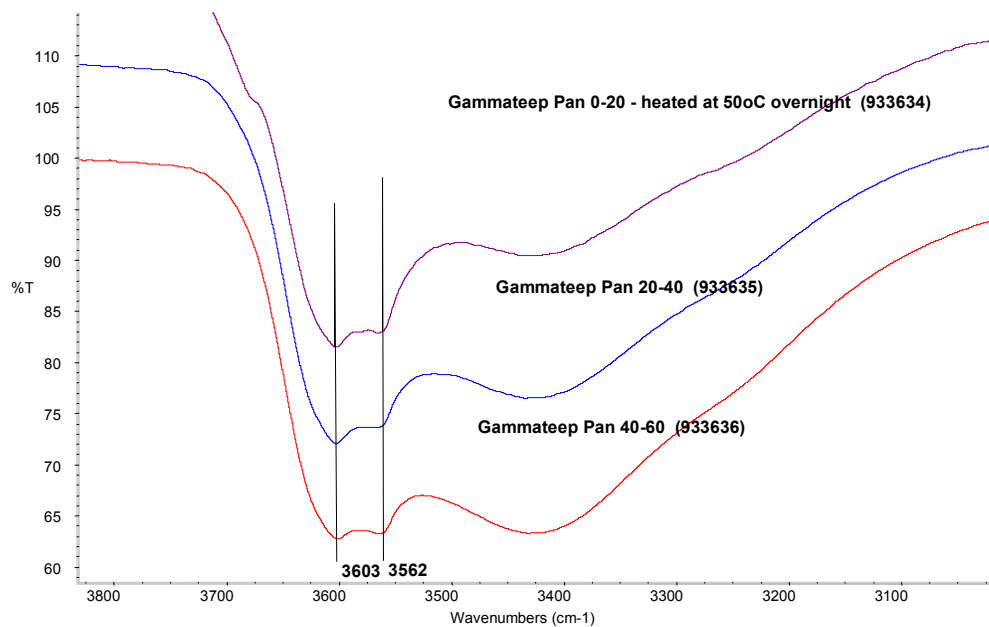
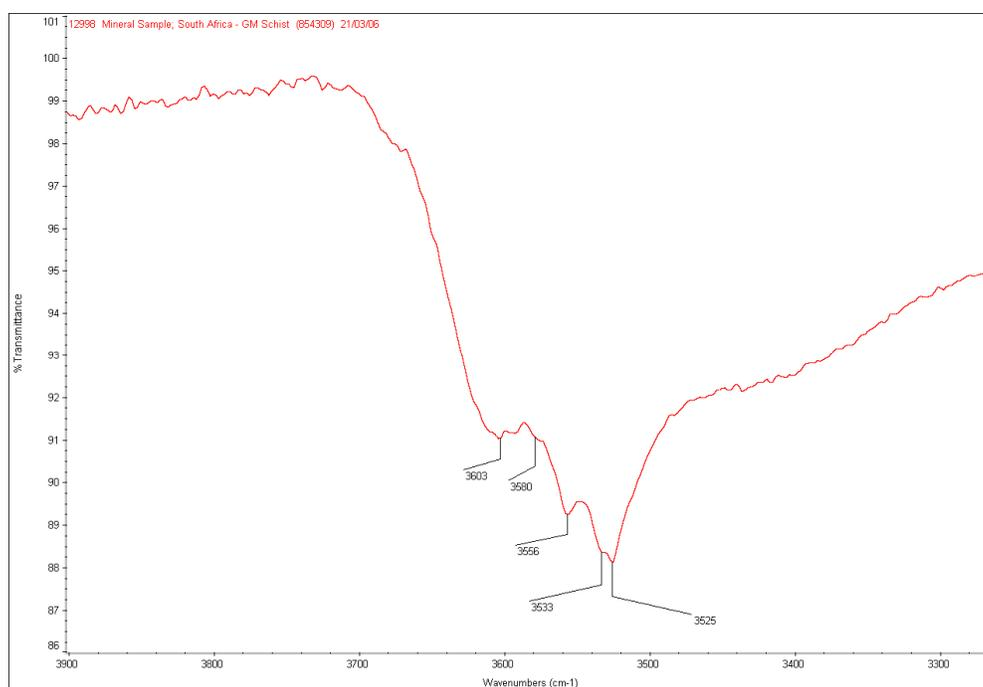


Figure 52. FTIR spectra in the OH stretching region for the Gammateep Pan samples

The frequency bands in the spectrum of the concentrated green clay are consistent with glauconite and/or celadonite. The strongest band is at  $3604\text{cm}^{-1}$  and corresponds to the AlMgOH stretch while a shoulder at  $3564\text{cm}^{-1}$  is slightly higher than previously observed at

3558  $\text{cm}^{-1}$ , in for example Koi Pan sediment, but corresponds to  $\text{Fe}^{3+}\text{MgOH}$ . A lower Fe system is suggested as the band at  $3534\text{cm}^{-1}$  ( $\text{Fe}^{3+}\text{Fe}^{2+}\text{OH}$ ) does not feature at all in the spectrum. A band is observed at  $837\text{cm}^{-1}$  and is attributed to celadonite. The possibility of the presence of some chlorite in the sample exists as the spectrum of iron-rich brunswigite has broad rounded peaks as seen at  $3434\text{cm}^{-1}$  and  $3565\text{cm}^{-1}$ .

The most intense band in the spectrum of the clay fraction from the green mica-schist, collected in a road that runs adjacent to Gammateep Pan, is at  $3525\text{cm}^{-1}$  and corresponded to  $\text{Fe}^{3+}\text{Fe}^{2+}\text{OH}$  observed for glauconite. The band observed at  $3580\text{cm}^{-1}$  is associated with celadonite and corresponds to  $\text{AlFe}^{2+}\text{OH}$ . The OH stretching region of the spectrum is illustrated in Fig. 53.



*Figure 53. FTIR spectrum of the clay fraction separated from the green mica-schist collected close to Gammateep Pan.*

### 5.6.3 Petrography and SEM

The sediment from Gammateep Pan is composed of fine-grained fragments of quartz and feldspar. The olive-brown matrix contains angular to sub-rounded grains of quartz and feldspar with minor amounts of mica and ilmenite. In Fig. 54 smectite set in a fine-grained matrix is shown and Fig. 55 shows a smectitic matrix hosting quartz grains. Some quartz grains appear to have quartz overgrowths. Quartz grains that show undulatory extinction (Fig. 56) are present suggestive of derivation from a source hosting strained quartz.



*Figure 54. Photomicrograph of a coarse-grained smectite set in a fine-grained clayey matrix. Auger sample taken from Gammateep Pan. Cross polarised light. Width of field of view 0.6mm.*

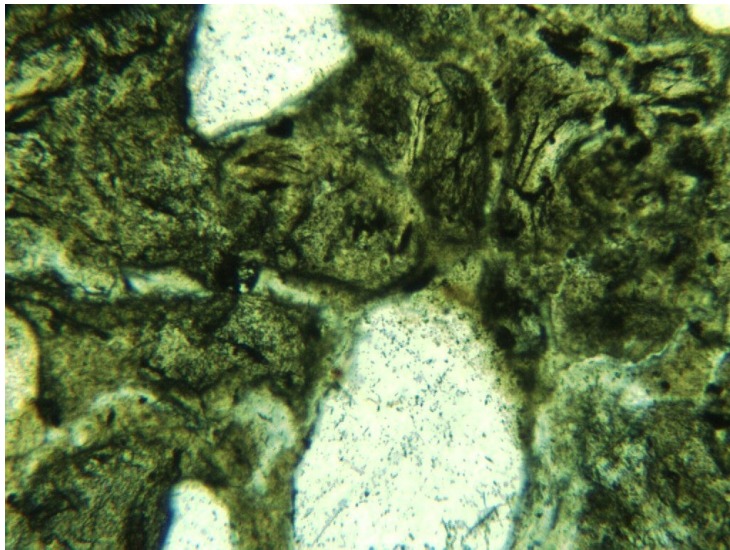


*Figure 55. Photomicrograph of a smectite matrix containing quartz grains in the Gammateep Pan sample. Plane polarised light. Width of field of view 0.6mm.*

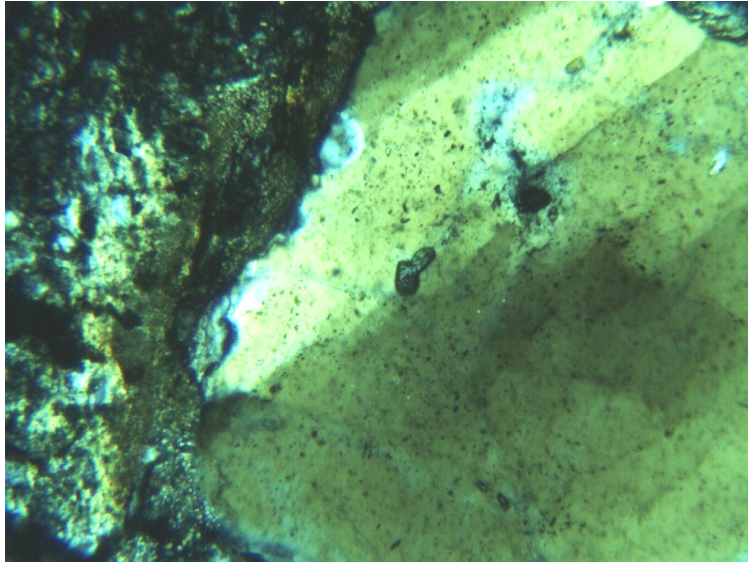


*Figure 56. Photomicrograph of the auger sample taken from Gammateep Pan showing a quartz grain with undulatory extinction. Cross polarised light. Width of field of view 0.6mm.*

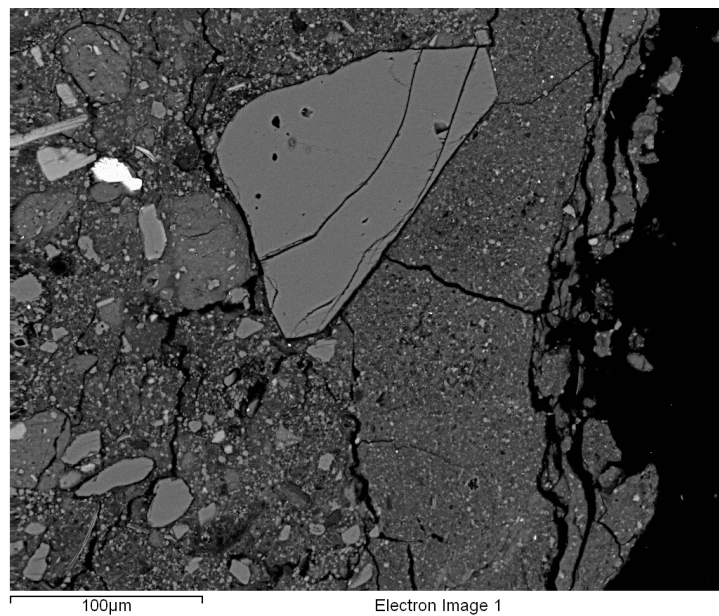


*Figure 57. BSE image of the sediment from Gammateep Pan showing grain size differences in the matrix.*

The BSE image showing the differences in the matrix of Gammateep Pan is shown in Fig. 57. Quartz grains varying in size are clearly visible in the matrix as well as an ilmenite grain, which appear white.

#### 5.6.4 XRF

The four profile samples and the sample of concentrated green clay were submitted for XRF analysis. The concentration of all oxides (Appendix D) appears to increase in a direction away from the surface, except for MgO and CaO, which decrease. Thus, the chemical analyses confirm the mineralogical results. In contrast with the other pans, positive correlations appear to exist between SiO<sub>2</sub>, Fe<sub>2</sub>O<sub>3</sub>, K<sub>2</sub>O and Na<sub>2</sub>O, while slightly negative correlations were observed for both MgO and CaO (Appendix D, Fig. D1).

Trace elemental analysis revealed that S occur in concentrations of between 0.63 and 0.14%. Other trace elements that occur at concentrations higher than 100ppm were; Sr, V, Zr and Ba.

#### 5.6.5 ICP-MS and IC

The water sample collected from the surface of the pan was submitted for chemical analysis and the results (Appendix E) show that the major solutes are Na, Ca and K with lesser quantities of Al and Mg. Cl<sup>-</sup> and SO<sub>4</sub><sup>2-</sup> are the dominant anions.

#### 5.7 Palaeo Molopo River bed

Green sandstone and shale, presumably from the Eden Formation, were sampled in the palaeo Molopo River bed.

##### 5.7.1 XRD

XRD results (Appendix B) indicate that the samples are dominated by dolomite (up to 77%) followed by quartz and minor amounts of mica, calcite, K-feldspar, plagioclase and illite/smectite interstratification.

##### 5.7.2 FTIR

The clay fraction of the sandstone was submitted for identification and the results are illustrated below in Fig. 58 and compared with the spectrum from Koi Pan sediment. Once again the most prominent band is seen at 3558cm<sup>-1</sup> and the presence of a tri-octahedral smectite is suggested for the sample. The mineralogical data together with the field observations suggest that this location might have been part of a pan-like environment at some stage.

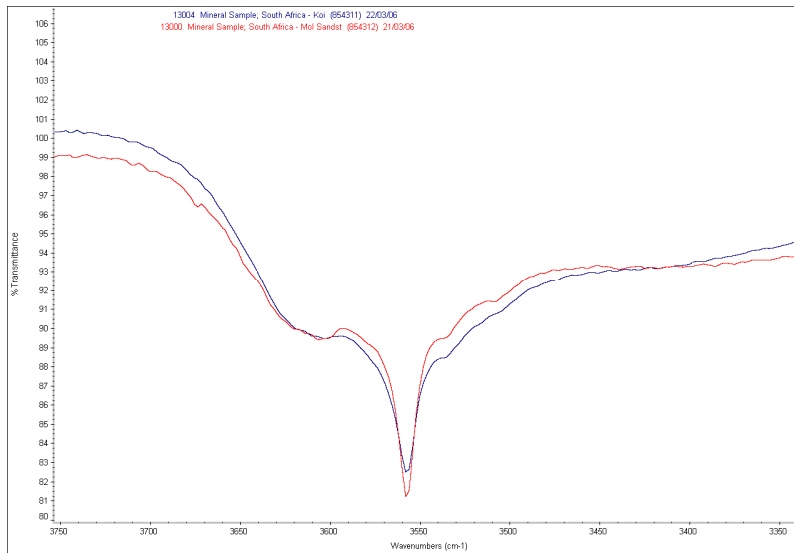


Figure 58. FTIR spectra of clay fractions from the sandstone as collected in the Palaeo Molopo River bed and pan sediment from Koi Pan.

#### 5.8 Additional data

The relative distribution of minerals is illustrated in Appendix B, Fig. B1 which show bubble plots of the XRD data for the study area. Similarly, in Appendix D, Fig. D2, bubble plots that illustrate the distribution of the major elements are presented.

#### Comparison between EDS analyses of areas in the fine-grained matrices from various pans

In Fig. 59, the  $K_2O/MgO$  ratios of areas in the matrices of the pan sediments are compared to ratios of standards (simultaneously analysed) and to data from the literature (Deer *et al.* 1996; Anthony *et al.* 1995). Brak Pan seems to have a fairly constant  $K_2O/MgO$  ratio that plots in line with the glauconite standard GLO, glauconite from Port Nolloth (PN) and glauconite from the literature. Some outliers with slightly higher Mg contents are observed but these appear to be in the range of the other pan's plots. In Fig. 60, the  $FeO/MgO$  ratios are shown and again the data from Brak Pan plot in a fairly straight line. Some of the data of Koi Pan plot in line with the Brak Pan data and some in a region with higher MgO values. The Gammateep Pan and Gai Gai Pan data plot in a region with higher MgO values. This higher MgO values coincides with higher dolomite percentages in the sediments.

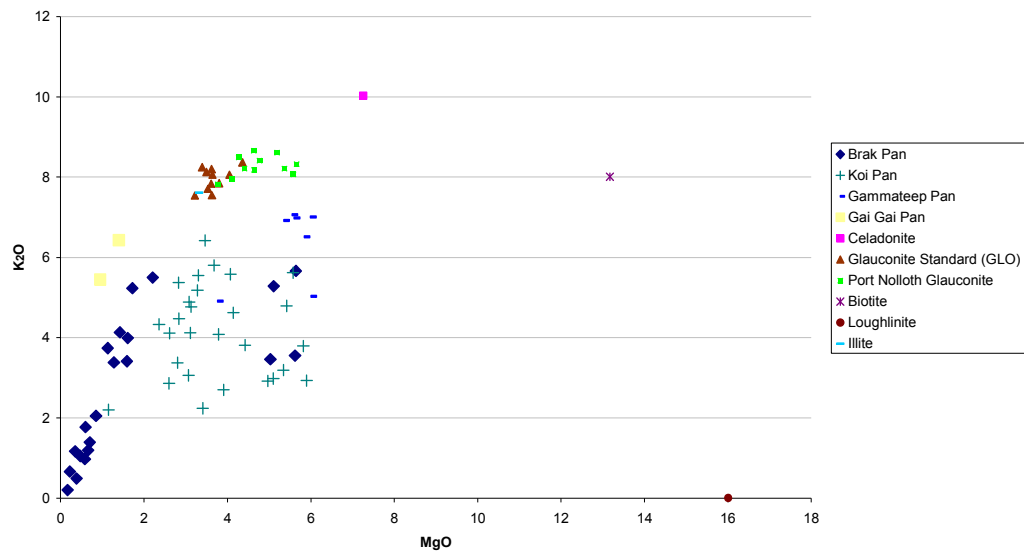


Figure 59. K<sub>2</sub>O versus MgO concentrations (in weight %) in the matrices from the various pans as compared with the compositions of selected minerals (from literature).

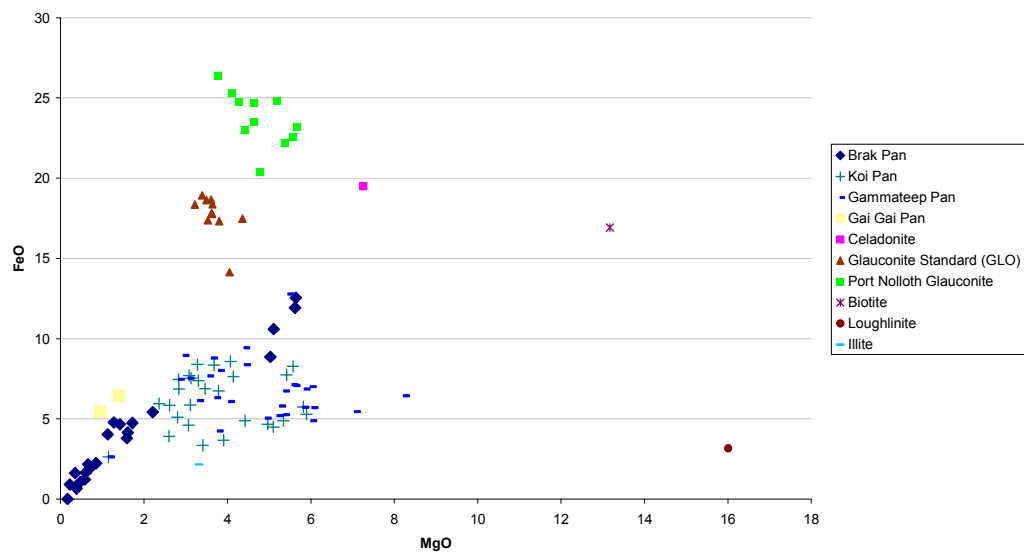


Figure 60. MgO versus FeO concentrations (in weight %) in the matrices from the various pans as compared with the compositions of selected minerals (from literature).

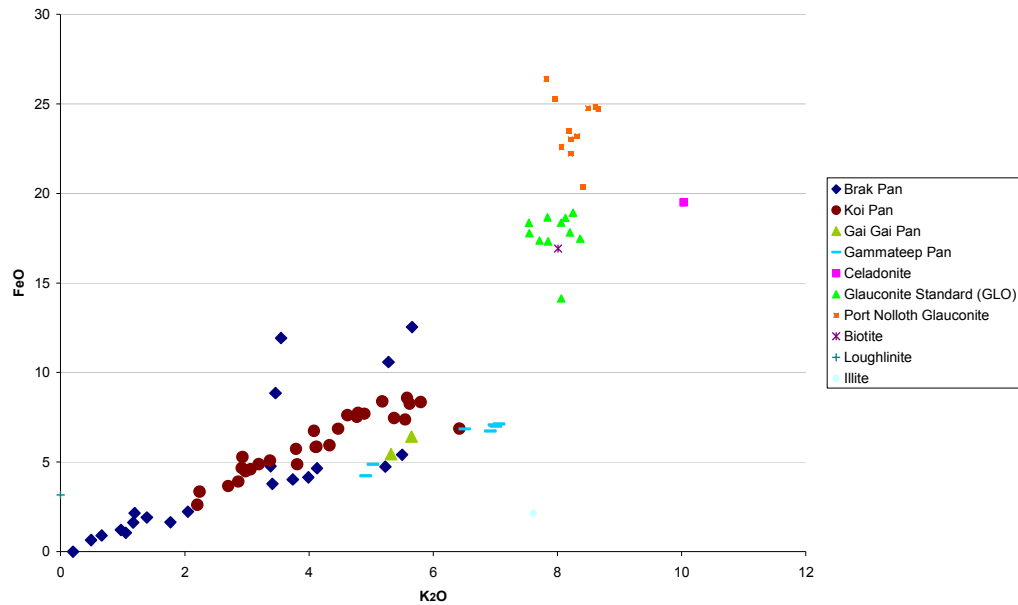


Figure 61.  $K_2O$  versus  $FeO$  concentrations (in weight %) in the matrices from the various pans as compared with the compositions of selected minerals (from literature).

Fig. 61 illustrates the relationship between FeO and K<sub>2</sub>O concentrations in the matrices of the pans. Most of the analysis for Brak Pan and Koi Pan plot along a fairly straight line towards the glauconite standard GLO, the Port Nolloth glauconite and glauconite values from the literature. However, the analyses for Gammateep and Gai Gai Pan show lower FeO values.

In Fig. 62 the ternary diagram shows FeO, K<sub>2</sub>O and MgO components of the matrices in the pans, the glauconite standard (GLO), marine glauconite from Port Nolloth, celadonite, biotite, loughlinite and illite from the literature as well as non-marine glauconite from the Karoo (Barton *et al.* 2004). The glauconite standard GLO, glauconite from Port Nolloth and non-marine glauconite from the Karoo compare very well, while the illite plot is off set. Most of the pan data seem to be richer in MgO and K<sub>2</sub>O than glauconite although the contribution of MgO bearing clays and even dolomite in some must be considered. If it is assumed that all or most of the K<sub>2</sub>O and FeO belong to mica in the matrix, then the compositions appear to broadly fall in a region close to glauconite and/or celadonite. However, some components with higher MgO and lower FeO are also evident.

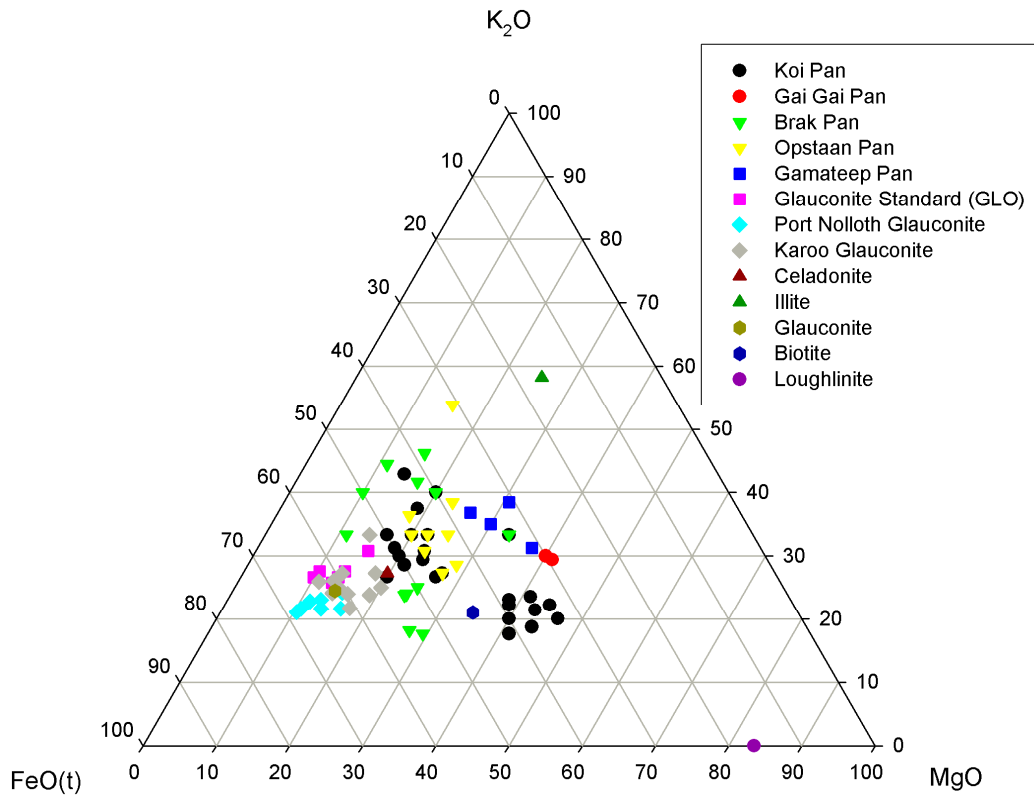


Figure 62. Ternary plot of MgO, FeO and K<sub>2</sub>O for the matrices in the various pan sediments (glauconite standard, Karoo glauconite, celadonite, loughlinite, biotite and illite from the literature).

## 6 Discussion

### 6.1 Koi Pan

The colour changes in the Koi Pan profile sediment are large, with a yellow-brown matrix becoming increasingly darker green with depth. XRD studies of the clay fraction of the sediment identified mica, loughlinitite and a small percentage of kaolinite and/or chlorite with the percentage mica remaining around 8% throughout the profile, although the percentage loughlinitite declined in a downward direction. FTIR identified the mica in the sediment as glauconite and/or celadonite and since very little mica could be identified under the microscopes it is deduced that the glauconite and/or celadonite forms part of the fine-grained matrix. The colour change at depth may in part be due to the mica being diluted by the loughlinitite in the shallow samples. High concentrations (up to 44%) of analcime are identified by XRD, but as this mineral is not recognised optically, it probably forms part of the fine-grained matrix. SEM EDS analyses of selected areas of the matrix were performed to determine the chemical constituents and how they vary. As seen from the BSE images, the matrix hosts a fine-grained fraction of the minerals previously reported, and even though areas were chosen with the least obvious interference from these minerals the possible contributions from them to the data must be considered.

The main chemical constituents comprising the matrix are  $\text{SiO}_2$ ,  $\text{MgO}$ ,  $\text{FeO}$ ,  $\text{K}_2\text{O}$  and  $\text{Na}_2\text{O}$ . Since  $\text{K}_2\text{O}$ ,  $\text{FeO}$  and some of the  $\text{MgO}$  can be attributed to the glauconite and/or celadonite, the three profile samples are considered in the  $\text{MgO}$ ,  $\text{FeO}$  and  $\text{K}_2\text{O}$  system (Fig. 63) and were compared to SEM EDS analyses of the glauconite standard GLO and a celadonite value from the literature.

Koi Pan sediment at a depth of 0-30cm below the surface show higher  $\text{MgO}$  values while the  $\text{K}_2\text{O}$  and  $\text{FeO}$  values increase at depth.

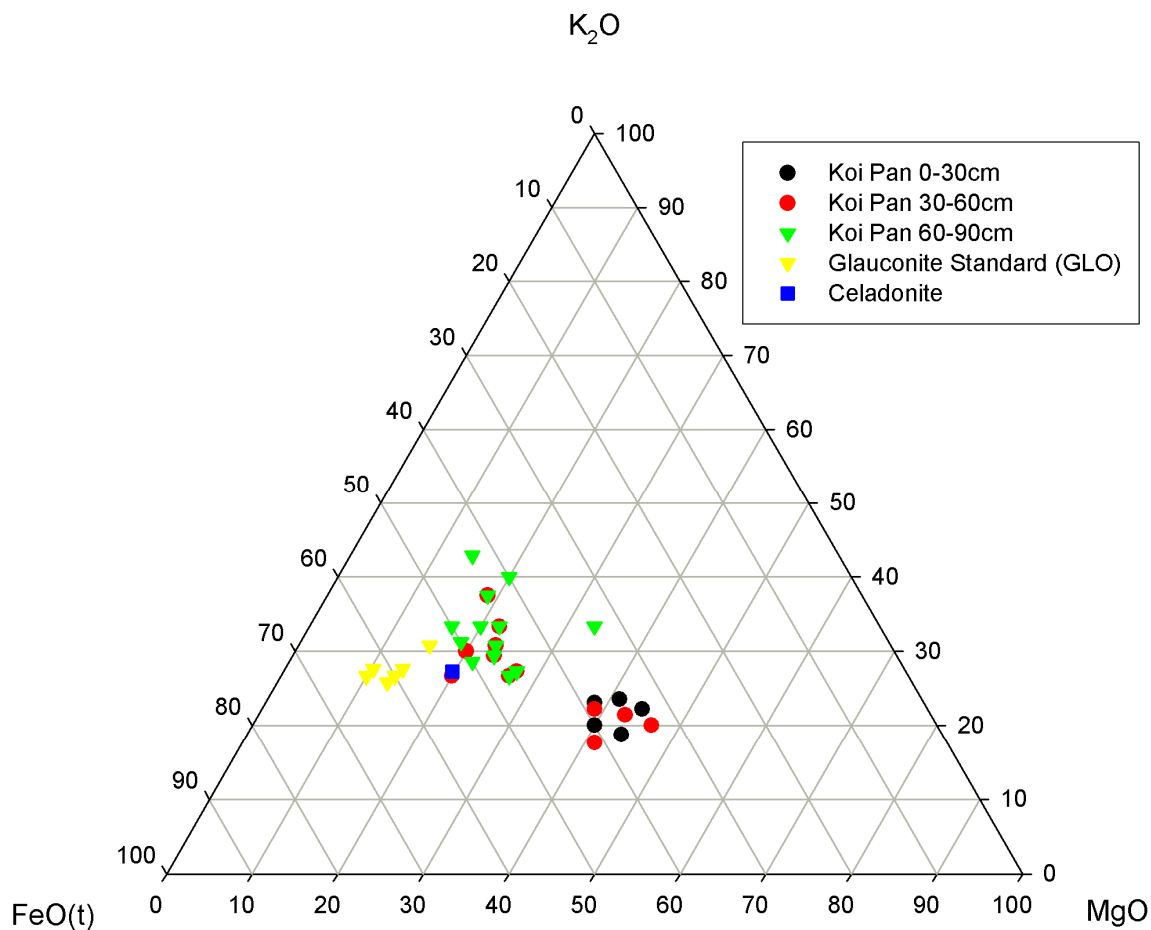


Figure 63. Ternary diagram for MgO, K<sub>2</sub>O and FeO (as normalised weight percentage) as present in Koi Pan sediment matrices.

Some of the data of Koi Pan 30-60cm, and to a lesser extent that of Koi Pan 60-80cm also plot in the higher MgO region. This might be due to infilling of desiccation cracks by the matrix that is less green (cf. Fig. 23). XRD data indicate that the dolomite content increases at depth and this may explain the MgO concentration being lower, in the clay matrix, at the contact with some dolomitic material. Furthermore, K<sub>2</sub>O and FeO values increase suggesting that MgO is extracted from the matrix to form dolomite leaving a matrix that is richer in FeO and K<sub>2</sub>O, the composition of which lies closer to Fe-celadonite. FTIR data tie in well with the ternary plot and indicate the presence of glauconite and/or celadonite throughout the profile, with only the Fe-celadonite component increasing in the deeper samples. The FTIR data argue for an Fe-rich celadonite that is poor in Al. Two analyses of the deepest sample, plot out of range and are considered to be areas where analcime dominate. The sepiolite identified by means of XRD could not be verified

with FTIR as the data is insufficient. It is only evident that some trioctahedral species are present in the Koi Pan 0-30cm sample producing a frequency intermediate between talc and sepiolite.

The bulk chemistry of the samples supports the mineralogical data and magnesium concentrations that increase in an upward direction are mostly associated with the occurrence of loughlinite. The absence of thenardite and loughlinite in the green sediment that represents older pan material, on the pan walls, suggest that these are authigenic minerals, currently forming in the pan. Because the mineral assemblage of the wall sediment does not include thenardite and loughlinite, but still has a green colour, it is suggested that these minerals play no role in the development of the glauconite and/or celadonite.

The formation of sepiolite in calcretes from the Kalahari has been reported by Netterberg (1969), Watts (1980) and other authors. It is suggested that the loughlinite forms after precipitation of low Mg calcite leading to Mg enrichment of the fluids that in turn lead to loughlinite formation.

## 6.2 Gai Gai pan

In comparison to Koi Pan, Gai Gai Pan differs mainly by having a higher abundance of quartz; also only mica, kaolinite and/or chlorite and smectite are identified in the clay mineral assemblage. Quartz appears to dilute the remaining minerals as positive correlations are observed between all elements apart from SiO<sub>2</sub>. This might indicate a higher mobility of the dune sand or that Gai Gai Pan is a younger generation pan.

The fine-grained matrix, as seen with the SEM, which hosts mostly grains of quartz is composed of SiO<sub>2</sub>, MgO, FeO, K<sub>2</sub>O and Na<sub>2</sub>O. Variations in the chemical distribution of these elements are observed in a cove created by an irregular shaped quartz grain filled by the fine-grained material. The high concentration of MgO in the region closest to the quartz grain followed by concentration of K<sub>2</sub>O and FeO in the matrix in contact with the area of elevated MgO concentration suggests some relationship between these elements - possibly the glauconite and/or celadonite formation, as the FeO and K<sub>2</sub>O concentrations in the matrix are attributed to glauconite and/or celadonite. The majority of the clay fraction from Gai Gai Pan comprise of an Fe-rich celadonite (as shown by FTIR) as was the case for Koi Pan.

## 6.3 Brak Pan

Mineral assemblages remain roughly the same as in Koi Pan, but dolomite occurs in lower

abundances while halite concentrations are higher. The loughlinites identified in Brak Pan might have formed by the same mechanism as suggested for Koi Pan, although no, or very little, dolomite is detected. It is also noted that loughlinites occur in concentrations below 5%. Brak Pan sediment is composed of essentially two types of material, the one occurring as discrete domains hosting fine-grained material, some showing veins of analcime, and with Mg occurring only in very low concentrations. These domains are correlated with the aggregates observed throughout the vertical profile of the pan sediment. The matrix that hosts these domains contains MgO in contrast to the aggregates, where MgO is absent. The matrix further hosts detrital quartz and a coarse-grained fraction of minerals. It is therefore suggested that the aggregates may be part of palaeo pan sediments reworked by the more recent MgO carrying pan sediment, and that it is currently undergoing alteration. FTIR analyses of the clay fraction of the aggregates show that illite is the dominant clay species, with only a trace of celadonite (probably as altered in the pan). The clay fraction of the matrix hosting the aggregates shows glauconite and/or celadonite in both the green and grey components into which the clay fraction separates. However, illite is the dominant clay in the grey component. The fact that the clay fraction from the matrix separates into two components that are distinct in colour – the one the same grey as the clay fraction of the aggregates and also dominated by illite, with some celadonite/glauconite character, supports the theory that the domains, or aggregates, are being reworked and also suggests that the glauconite and/or celadonite and illite are dissociated. Overall the clay fractions from Brak Pan show a less dominant celadonite component than that observed in Koi Pan.

Although the TL samples were taken at approximately the same depth in Brak Pan and Koi Pan there is quite a large difference in their ages (~141ka versus ~42ka). This suggests different sedimentation rates or that Brak Pan is much older than Koi Pan. The sample taken at 184cm below the surface of Brak Pan is older than 150ka.

#### 6.4 Opstaan Pan

The Opstaan Pan sediment is much more reddish brown in colour compared to the other pans, and the overall grain size much finer. The mineral assemblage is generally the same as in the other pans with dolomite and thenardite barely featuring. The main clay minerals are mica, smectite and kaolinite and/or chlorite. The matrix of the sediment has two distinguishing features: 1) the colour differences that varies between red-brown and yellow-brown and 2) the chemical variation that mainly involve  $\text{Na}_2\text{O}$ ,  $\text{Al}_2\text{O}_3$  and  $\text{SiO}_2$ . Overall Opstaan Pan appears to be less mature than Brak Pan and Koi Pan, lacking the dark olive-green sediments. FTIR data indicate the presence of

celadonite and/or glauconite but the absorptions were relatively less intense than that of Koi Pan.

#### 6.5 Sout Pan

The Sout Pan sediment is extremely brackish compared to the other pans with halite being the main mineral component in the two profile samples. The clay minerals mica, and kaolinite and/or chlorite are present in the pan sediment. The high salt content makes chemical and microscope investigations extremely difficult and the sediment samples were not analysed further. Chemical analysis of the water sample obtained from the auger hole is dominated by Na followed by Ca. The anions are, as expected, mostly  $\text{Cl}^-$ .

#### 6.6 Gammateep Pan

The Gammateep Pan sediments have the same mineral assemblages found in the other pans, but a notably lower salt content and no analcime. FTIR data indicate the presence of glauconite and/or celadonite but suggests a lower Fe system with the Fe content increasing in a downward direction for the profile samples. It is significant that the concentrated green clay sample is the only sample in which halite is identified. Where mica occurs at its highest concentration the FTIR features of glauconite and/or celadonite are most readily visible. The water sample is, as in the case of Sout Pan, dominated by Na and  $\text{Cl}^-$  but to a lesser extent.

## 7 Conclusions

This study provides information on the mineralogy (particularly the clay minerals) and geochemistry of pans situated in the Northern Cape Province. From the east to west the abundance of salt (halite and thenardite) in the pans increases and with it the intensity of the green colour of the sediment. The salt content is associated with the physical maturity or possibly the age of the pans, as those to the west are deeper and wider compared to the pans to the east such as Gammateep Pan. Authigenic calcite, dolomite, analcime and loughlinite (Na-sepiolite) occur in some of the pans to the west and clay mineralogy shows that all the pans host glauconite and/or celadonite but smectite, illite/smectite interstratification, smectite and kaolinite and/or chlorite and loughlinite only occur in some. Chemically the bulk sediments are dominated by  $\text{SiO}_2$  that also acts as a dilutant for  $\text{Fe}_2\text{O}_3$ ,  $\text{K}_2\text{O}$ ,  $\text{NaO}$ ,  $\text{Al}_2\text{O}_3$  and in some cases  $\text{MgO}$  concentrations in all the pans but Gammateep Pan.  $\text{Fe}_2\text{O}_3$  concentrations correlate well with trends in the mica abundances while dolomite correlates with  $\text{MgO}$  values and especially in the pans where little or no halite is present analcime correlates with  $\text{Na}_2\text{O}$  values.

The glauconite and/or celadonite does not occur as discrete mineral grains, but forms part of the fine-grained matrix common in all of the pans. Chemical variation identified by FTIR in the composition of the glauconite and/or celadonite included enhanced absorption bands of Fe-celadonite in some pans to the west (such as Koi Pan and Gai Gai Pan) while a lower Fe system was apparent in Gammateep Pan (situated to the east of the study area). Overall the FTIR bands most clearly recognised are those of celadonite – especially in the more mature pans.

Colour differences in the matrix of the Koi Pan sediment are associated with variations in the  $\text{K}_2\text{O}$ ,  $\text{FeO}$  and  $\text{MgO}$  concentrations in the clay matrix. This is also associated with an increase in the celadonite bands (FTIR) present in the matrix and a decrease in the loughlinite abundance (XRD) at depth. It is suggested that the loughlinite found in Koi Pan is authigenic, and forms after precipitation of low Mg calcite (confirmed with XRD) leading to Mg enrichment of the fluids and subsequent loughlinite formation with minor dolomite. The loughlinite identified in Brak Pan might have formed by the same mechanism although no dolomite was detected by XRD. The aggregates found throughout this pan's profile have illite as the main clay mineral while the matrix separates into two distinct layers: one glauconite and/or celadonite-rich and the other illite-rich. This suggests that the two clays exist separately and that the aggregates are being reworked by the pan processes.

An interesting feature in Gai Gai Pan was a fractured quartz grain filled by the fine-grained matrix. FeO and K<sub>2</sub>O appear to substitute for MgO or *vice versa* in this shielded area (cf. Fig. 35). Considering the literature report (McRae 1972) which state that glauconite sometimes develops in shells that provide a micro environment, it is suggested that the processes that are active in the pans are enhanced by micro environments and the co-formation of specific minerals as is the case for glauconite.

As the Vryheid Formation is not reported to occur in the study area it is considered that no source of glauconite exists in the surrounding geology. Glauconite and/or celadonite in a pan environment with no known source of marine glauconite or igneous rocks for celadonite are anomalous. In order to hypothesize how this clay formed in a terrestrial environment Table 5, showing facts and some similarities between the studied Kalahari glauconite and/or celadonite, and glauconite and celadonite, is presented. The data is based on information reported by Odin (1988). It is considered that the pan environment presents a closed, saline setting that provides conditions such as high pH and both oxidising and reducing settings (as the water-table seasonally fluctuates). Slow to no sedimentation rates and fluids that interact with the chemical immature Dwyka diamictite to yield ion-rich brines when water circulates also contributes to make this environment ideal. The water table reaches the surface of Brak Pan (salt abundance is highest in the crust sample) and this ensures that sediment of the whole profile is exposed to the ion enriched brines causing the whole profile to become green. In contrast to Brak Pan, Koi Pan contains sediment that intensifies in green colour with depth, with the salt content being highest in the greenest sample. This suggests that the water-table has only reached up to 60-80cm below the surface and only the sediment that was exposed to it was altered. Like wise the sediments from Gammateep Pan and Opstaan Pan show a positive correlation between salt content, percentage mica and green colouration. The influence of the water-table on the formation of the glauconite and/or celadonite thus appears to be most significant as the highest abundance of salt is always associated with the position in the profile where the sediment appears to reach its most intense green colour. No evidence was found for a precursor mineral from which the glauconite and/or celadonite develops during either the XRD or microscopy investigations. According to Table 5, celadonite precipitates as microcrystals in a single reaction while in equilibrium with the circulating fluids, while glauconite formation usually involves a precursor mineral and forms larger microcrystals. However, Odin and Fullagar (1988) concluded that nearly all components of sediment may become green provided that they are in granular form, and that no mineralogically similar substrate is necessary for glauconitization to occur. The FTIR analysis of the clay fraction

of the conglomerate's (grit) green alteration zone sampled in Gai Gai Pan shows the same glauconite and/or celadonite found in the pan sediment. Since the glauconite and/or celadonite occurs as part of fine-grained material and because formation appears to be associated with the present day position of the water-table it is suggested that the glauconite and/or celadonite are authigenic and possibly still forming under the present conditions.

The green alteration rim of the conglomerate (grit) and sandstone found in Gai Gai Pan leads to the conclusion that in, and close to, the pans the water-table circulates ion rich brines that leads to the formation of a mica which composition lies between glauconite and celadonite, and in most cases more to the side of celadonite. The dessication cracks associated with green shale and sandstone that were found in the palaeo Molopo Riverbed might suggest that they also formed in a pan-like environment.

The association of celadonite with zeolites is also of importance as analcime is thought to be authigenic in the pans to the west. No analcime was found in Gammateep Pan but the pan appeared immature in comparison to the pans in the west, has a very low salt content and its FTIR data show it to be lower in iron content.

The discrepancy in the ages of pan sediment taken at roughly the same depth in Koi Pan and Brak Pan might suggest different sedimentation rates. However, it might also suggest much younger ages or faster formation for glauconite and/or celadonite in Koi Pan since it is suggested that the mineral is authigenic. The possibility also exists that the younger age from Koi Pan might be as a result of reworked glauconite and/or celadonite (from the edges of the pan) as this pan seems to be expanding at present (cf. Fig. 13).

Table 5. A comparison between the environments and conditions of formation for glauconite, celadonite and the Kalahari glauconite/celadonite

<b>Glauconite</b>	<b>Kalahari glauconite and/or celadonite</b>	<b>Celadonite</b>
<i>Physical environment</i>		
saline	saline	saline
slow sedimentation rates	slow sedimentation rates	deep sea
below 15°C or even 10°C	3°C - > 35°C	20°C (50-90°C)
pH 7-8	pH 9-10	
oxidising and reducing conditions in presence of organic material	oxidising and reducing (seasonal), organic material present	oxidising and reducing conditions
shells provide closed environment with local reducing conditions	pan provides closed environment	needs confined spaces to minimized dilution of fluids
concentrated on continental shelf areas, fairly shallow waters, from variety of starting material by marine diagenesis	shallow water (seasonal) no substrate noticed	from volcanic rock at sea bottom
<i>Chemical environment</i>		
availability of K and Fe in pore fluids, sea water travel short distance ~ sea water composition not changed much	situated on weathering Dwyka diamictite, water table shallow- [salt] increases from bottom to surface	grow from very ion rich fluids- sea water travel deep through fractures and are modified by rock before reaching the void where mineral precipitate
form from successive reactions: Fe-rich smectite-recrystallization processes which trap more and more K	no indication of solid solution between mica and smectite	forms in equilibrium with circulating fluid in a single reaction
develops in micropores from substrate	develops as matrix of pan sediment	develops in voids
microcrystals larger; occur as grains	fine-grained matrix of pan sediment	microcrystals smaller; never occur as grains
<i>Associated minerals</i>		
no association with zeolites	analcime, smectite in some pans	associated with smectite and zeolites

## **8 Acknowledgements**

The project was proposed by Dr Frank Netterberg as a modern and detailed follow up on his earlier work finding what appeared to be glauconite in many areas of the Kalahari. Thanks to Dr M. Cloete for his contributions especially during the initiation of the project and for accompanying me to the Kalahari.

Special thanks to the Council for Geoscience that allowed and funded this project as part of their statutory research program. Thank you Professor Dunlevey for the time you have spent on this thesis and for financially supporting this project.

Natuurlik die meeste dank aan ons Almagtige Skepper wat alles so perfek en interessant gemaak het! Dankie Mamma en Pappa dat julle my altyd en in al my ondernemings ondersteun. Aan my skoonma en skoonpa baie dankie vir julle ondersteuning - veral deur Carlyn en Rainhard op te pas as ek moes werk.

Dankie Freddie, Carlyn en Rainhard – julle is deel van elke motivering en oorweging in my lewe.

## 9 References

- Anthony J.W., Bideaux R.A., Bladh K.W. and Nichols M.C., 1995. Handbook of mineralogy, vol. 2. Mineral data publishing, 904 pp.
- Bailey, S.W., 1980. Structures of layer silicates. In: Crystal structures of clay minerals and their X-ray identification (Brindley, G.W. and Brown, G. eds.). Mineralogical Society Monograph no. 5, p 1-124.
- Barton, J.M. (Jr.), Cairncross, B. and McLachlan, I., 2004. Rb-Sr Isotopic and elemental studies of the origin of glauconite in the Permian northern coal fields, South Africa: Evidence for a thermal Mid-Jurassic influence. *South African Journal of Geology* 109: 499-504.
- Bates, R.L. and Jackson, J.A., 1983. Dictionary of geological terms, 3<sup>rd</sup> ed. American Geological Institute, 571 pp.
- Bentor, Y.K. and Kastner, M., 1965. Notes on the mineralogy and origin of glauconite, *Journal of Sedimentary Petrology* 35: 155-166.
- Birch, G.F., Willis, J.P. and Rickard, R.S., 1976. An electron microprobe study of glauconites from the continental margin off the west coast of South Africa, *Marine Geology* 22: 271-283.
- Boocock, C. and Van Straten, C.J., 1962. Notes on the geology and hydrogeology of the Central Kalahari region, Bechuanaland Protectorate. *Transactions of the Geological Society of South Africa* 65: 125-171.
- Brime, C., 1985. The accuracy of X-ray diffraction method for determining mineral mixtures, *Mineralogical Magazine* 49: 531-538.
- Buckley, H.A., Bevan, J.C., Brown, K.M., Johnson, L.R. and Farmer, V.C., 1978. Glauconite and celadonite: two separate mineral species. *Mineralogical Magazine* 42: 373-382.
- Buhmann, D., Gabrielli, F. and Netterburg, F., 1999. A glauconite, green-illite, smectite and sepiolite sequence from the Heuningvlei Pan, North West Province, South- Africa. Abstract Volume, p. 67, Conference on the European Clay Groups Association, Euroclay 1999, 5-9 September 1999, Krakow, Poland.
- Burst, J.F., 1958. Mineral heterogeneity in "glauconite" pellets. *The American Mineralogist* 43: 481-497.
- Cadle, A.B., 1995. Depositional systems of the Permian Vryheid Formation, Highveld coalfield, South Africa. Their relationship to coal sea, occurrence and distribution. Unpublished PhD thesis, University of Witwatersrand, 316 pp.
- Cornell, D.H., Thomas, R.J., Moen, H.F.G., Ried, D.L., Moore, J.M., and Gibson, R.L., 2006. The Namaqua-Natal province. In: The geology of South Africa (Johnston, M.R.,

- Anhaeuser, C.R. and Thomas, R.J. eds.). Geological Society of South Africa, Johannesburg, 691 pp.
- Deer, W.A., Howie, R.A. and Zussman, J., 1996. *An introduction to the rock forming minerals*, 2nd edition, 695 pp.
- Du Toit, A., 1954. Geology of South-Africa, 3<sup>rd</sup> Edition, Edinburgh, 611 pp.
- Ehlmann, A.J., Hulings, N.C. and Glover, E.D., 1963. *Journal of Sedimentary Petrology* 33: 87-96.
- Eugster, H.P. and Kelts, K., 1983. Lacustrine sediments. In: Chemical sediments and geomorphology, precipitates and residua in the near-surface environment (A.S. Goudie and K. Pye eds.). Academic Press Inc. London Ltd, 439 pp.
- Fahey, J.J., Ross, M. and Axelrod, J.M., 1960. Loughlinite, a new hydrous sodium magnesium silicate. *The American Mineralogist* 45: 270-281.
- Goudie, A.S. and Thomas, D. S., 1985. Pans in Southern Africa with particular reference to South Africa and Zimbabwe. *Zeitschrift fuer Geomorphologie* 29: 1-19.
- Gruner, J.W., 1935. The structural relationship of glauconite and mica, *American Mineralogist* 20: 699-714.
- Hagelskamp, H.H.B., 1987. The influence of depositional environment and dolerite intrusions on the quality of coal, a study of Twitsdraai Mine area near Secunda, south-eastern Transvaal. Unpublished PhD thesis, University of Pretoria, South Africa, 272 pp.
- Hendricks, S.B. and Ross, C.S. 1941. Chemical composition and genesis of glauconite and celadonite, *The American Mineralogist* 26: 683-708.
- Huggett, J.M. and Laenen, L., 1996. Green clays from the lower Oligocene of Aardebrug, Belgium: A re-evaluation, *Clay Minerals* 31: 557-562.
- Hillier, S., 1995. Erosion, sedimentation and sedimentary origin of clays. In: Origin and mineralogy of clays, Clays and the Environment (B. Velde ed.), Springer Verslag Berlin, Germany, 162-219.
- Hower, J., 1961. Some factors concerning the nature and origin of glauconite, *The American Mineralogist* 46: (1-6) 313-334.
- Jarrar, G., Amirehh, B. and Zachmann, D., 2000. The major, trace and rare earth element geochemistry of glauconites from the early Cretaceous Kurnub Group of Jordan, *Geochemical Journal* 34: 207-222.
- Keller, W.D., 1958. Glauconitic mica in the Morrison Formation in Colorado. *Clays and Clay Minerals* 5: 120.
- Kossovskaya, A.G. and Drits, V.A., 1970. The variability of micaceous minerals in sedimentary

- rocks. *Sedimentology* 15: 83-101.
- Malherbe, S.J., Keyser, A.W., Botha, B.J.V., Cornelissen, M.A., Slabbert, M.J. and Prinsloo, M.C., 1986. The tertiary Koa River and the development of the Orange River drainage. *Annals of the Geological Survey of South Africa* 20: 13-23.
- Manghnani, M.H. and Hower, J., 1964. Glauconites: Cation exchange capacities and infrared spectra, *American Mineralogist* 49: 586-598.
- McRae, S.G., 1972. Glauconite. *Earth-Science Review* 8: 397-440.
- Mees, F., 2001. An occurrence of lacustrine Mg-smectite in a pan of the southwestern Kalahari, Namibia. *Clay Minerals* 36: 547-556.
- Mees, F., 2003. Salt mineral distribution patterns in soil of the Otjomongwa pan, Namibia. *Catena* 54: 425-437.
- Millot, G., 1970. *Geology of clays*. Translated by W.R. Farrand and H. Paquet, Springer-Verlag.
- Moore, D.M. and Reynolds, R.C. (Jr.), 1997. X-ray diffraction and the identification and analysis of clay minerals, 2nd edition, Oxford University press, 378 pp.
- Netterberg, F., 1969. The geology and engineering properties of South African Calcretes. Ph.D thesis, University of the Witwatersrand, 1 070 pp.
- Odom, I.E., 1984. Glauconites and celadonite minerals. In: *Micas* (Bailey, S.W. ed.). *Review in mineralogy* 13, Mineralogical Society of America, Washington, D.C., 545-572.
- Odin, G.S. and Matter, A., 1981. De glauconiarum origine. *Sedimentology* 28: 611-641.
- Odin, G.S., 1988. Glaucony from the Gulf of Guinea. In: *Green Marine Clays* (Odin, G.S ed.) *Developments in Sedimentology* 45: 225-247.
- Odin, G.S. and Fullagar, P.D., 1988. Geological significance of the glaucony facies. In: *Green Marine Clays* (Odin G.S ed.). *Developments in Sedimentology* 45: 295-332.
- Oosterhuis, W.R., 1998. Salt. In: *Mineral resources of South Africa* (Wilson, M.G.C. and Anhaeusser, C.R eds.). Council for Geoscience, Handbook 16, 584-586.
- Parry, W.T. and Reeves, C.C., 1966. Lacustrine mica from pluvial lake Mound, Lynn and Terry Counties, Texas. *The American Mineralogist* 51: 229-235.
- Porrenga, D.H., 1968. Non-marine glauconitic illite in the lower Oligocene of Aardebrug, Belgium, *Clay Minerals* 7: 421 – 430.
- Rieder, M., Gavazzini, G., D'yakonov, Y.S., Frank-Kamenetskii, V.A, Gottardi, G., Guggenheim, S., Koval, P.V., Muller, G., Neiva, A.M.R., Radoslovich, E.W., Robert, J., Sassi, F.P., Takeda, H., Weiss, Z. and Wones, D.R., 1998. Nomenclature of micas. *The Canadian Mineralogist* 36: 41-47.
- Rogers, A.W., 1937. The surface geology of the Kalahari. *Transactions of the Royal Society of*

- South Africa* 24: 57-80.
- Schmidt, E.R., 1976. Clay. In: Mineral resources of South Africa (Wilson, M.G.C. and Anhaeusser, C.R. eds.). Council for Geoscience, Handbook 7, Geological Survey, Pretoria, 275-288.
- Slonimskaya, M.V., Besson, G., Dainyak, L.G., Tcoubar, C. and Drits, V.A., 1986. Interpretation of the IR spectra of celadonites and glauconites in the region of OH-stretching frequencies. *Clay Minerals* 21: 377-388.
- South African Committee for Stratigraphy (SACS), 1980. *Stratigraphy of South Africa Part 1: Lithostratigraphy of the Republic of South Africa, South West Africa / Namibia and the Republics of Bophutatswana, Transkei and Venda*. (Kent, L.E., Compiler) Handbook of the Geological Survey of South Africa 8. Government Printer, Pretoria.
- Srodon, J. and Eberl, D.D., 1984. Illite, Chapter 12, 495-539. In: Micas (Bailey, S.W. ed.). *Review in Mineralogy* 13, 584 pp.
- Thomas, D.S.G. and Shaw, P.A., 1989. Playas, pans and salt lakes. In: Arid zone geomorphology (Thomas, D.S.G. ed.), 363 pp.
- Thomas, D.S.G. and Shaw, P.A., 1991. The Kalahari environment. Cambridge Univ. Press, 284 pp.
- Thomas, R.J., Thomas, M.A. and Malherbe, S.J., 1988. The geology of the Nossob and Twee Rivieren areas, Explanation of sheet 2520 and 2620, Geological Survey, South Africa.
- Thomas, R.J. and Thomas, M.A., 1989. The geology of the Noenieput area, Explanation of sheet 2720, Geological Survey, South Africa.
- Velde, B., 1992. Introduction to clay minerals, Springer 1<sup>st</sup> edition, 195 pp.
- Weaver, C.E. and Pollard, L.D., 1973. The chemistry of clay minerals, *Developments in Sedimentology* 15: 25-45.
- Winter, M.F., 1985. Lower Permian palaeo-environments of the northern Highveld Coalfield and their relationship to the characteristics of coal seams. Ph.D. thesis (unpublished), University of Witwatersrand, Johannesburg, 254 pp.